experimental curves at different low temperatures by the differential and combined integral techniques to compare to the recent theory developed by Blume and Tjon.[17]

[17] M. Blume and J. A. Tjon, Phys. Rev. 165, 446 (1968).

ACKNOWLEDGMENTS

One of the authors (P. da R. A.) thanks the Conselho Nacional de Pesquisas, Brasil, for a research lecturer fellowship and another (J. D. R.) is indebted to the Pan American Union for support during this work.

PHYSICAL REVIEW B VOLUME 1, NUMBER 7 1 APRIL 1970

Theory and Operation of Proton Spin Refrigerators: Sizable Proton Polarizations*

J. R. McColl† AND C. D. Jeffries
Department of Physics, University of California, Berkeley, California 94720
(Received 25 August 1969)

The enhancement of proton spin polarization by the spin-refrigerator method, in crystals of $Y(C_2H_5SO_4)_3 \cdot 9\,H_2O$ containing a few percent Yb^{3+}, is studied experimentally and theoretically. The spin refrigerator is operated simply by rotating the crystal in a magnetic field at liquid-helium temperatures, or by subjecting the crystal to a pulsed rotating field. The proton polarization comes about because the Yb spins have both anisotropic g value ($g_{\parallel}=3.4$, $g_{\perp}\approx 0$) and relaxation rate ($T_{1e}^{-1} \propto \cos^2\theta \sin^2\theta$), so the Yb spin polarization at $\theta=45°$ can be transferred by cross-relaxation to the protons at $\theta=90°$ by rapid rotation of the crystal or field between these two orientations. A unified theory involving electronic and nuclear spin-lattice relaxation, cross-relaxation, and nuclear spin diffusion explains the results of both types of spin refrigerator, and predicts that polarizations as high as 70% may be achieved at higher operating speeds. Proton polarizations as high as 35% are reported, suggesting application to polarized targets.

I. INTRODUCTION

RECENTLY, Langley and Jeffries[1,2] (LJ) have obtained proton polarizations as high as 19% using a nuclear-spin refrigerator,[3,4] and interpreted their results with a simple, phenomenological model. By extending their measurements and developing a new type of spin refrigerator involving pulsed rotating fields, we have obtained proton polarizations as high as 35% in crystals of $(^{172}Yb,Y)(C_2H_5SO_4)_3 \cdot 9H_2O$ (abbreviated as ^{172}Yb:YES). The new results are interpreted in terms of a microscopic theory which predicts that proton polarizations as high as 70% may be achieved under ideal experimental conditions. This polarization is high enough that the spin refrigerator is an interesting possibility for use in polarized proton targets, as an alternative to the dynamic microwave polarization method[5–7] presently being used.

To illustrate a type of pulsed field spin refrigerator, we consider a 1% Yb:YES crystal mounted in the apparatus of Fig. 1. The crystal is oriented with its c axis vertical in a liquid ^{4}He bath pumped to $\sim$1.2°K. A copper solenoid which produces a vertical pulsed field $\mathbf{H}_p \sim 15$ kOe of 200-μsec duration is placed in the liquid N_2 (LN) bath for cooling. The apparatus is in the field $\mathbf{H}_{dc}$ of a steel electromagnet capable of producing up to 20 kOe. The YES crystals are diamagnetic except for the Yb^{3+} ions, which behave like spins with $S=\frac{1}{2}$, but with the highly anisotropic g value

$$g^2(\theta)=g_{\parallel}^2 \cos^2\theta+g_{\perp}^2 \sin^2\theta, \quad (1)$$

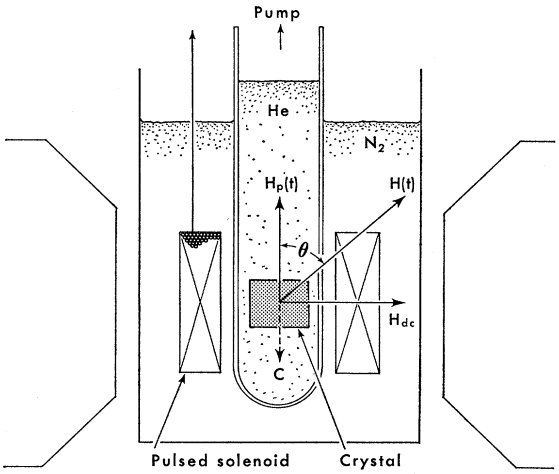

FIG. 1. Experimental arrangement for a pulsed-field spin refrigerator.

* Supported in part by the U. S. Atomic Energy Commission, Contract No. AT(11-1)-34, Project 20, Report No. UCB-34P20-139.
† NSF Predoctoral Fellow. Present address: Physics Department, Yale University, New Haven, Conn. 06520.
[1] K. H. Langley and C. D. Jeffries, Phys. Rev. Letters 13, 808 (1964).
[2] K. H. Langley, and C. D. Jeffries, Phys. Rev. 152, 358 (1966).
[3] C. D. Jeffries, Cryogenics 3, 41 (1963).
[4] A. Abragam, Cryogenics 3, 42 (1963).
[5] C. D. Jeffries, Phys. Rev. 106, 164 (1957); 117, 1056 (1960).
[6] A. Abragam and W. G. Proctor, Compt. Rend. 246, 2253 (1958).
[7] C. D. Jeffries, *Dynamic Nuclear Orientation* (John Wiley & Sons, Inc., New York, 1963).

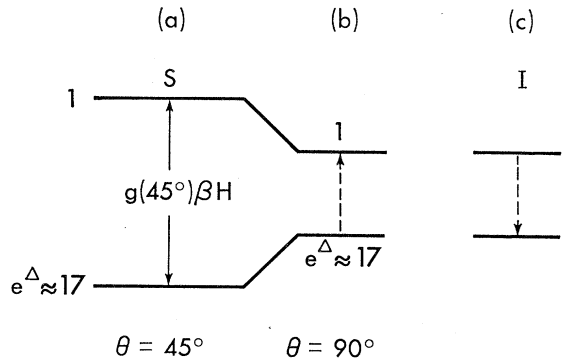

FIG. 2. (a) Magnetic energy level of Yb spin at $\theta=45°$, showing large difference in population due to large Boltzman factor; (b) energy level of Yb spin after isentropic passage to $\theta\approx90°$; (c) proton energy levels commensurate with Yb levels in (b) so that mutual spin flips may occur.

where[8] $g_{11}=3.4$ and $g_\perp\approx0$, and θ is the angle between the total magnetic field $\mathbf{H}=\mathbf{H}_{dc}+\mathbf{H}_p$ and the crystalline c axis. The numerous protons in the waters of hydration and ethyl radicals form a nuclear spin system with $I=\frac{1}{2}$, with isotropic g value $g_n=0.00304$, referred to the Bohr magneton μ_B. A vertical rf coil (not shown) is wound around the crystal to measure the NMR signal, which is just proportional to the proton spin polarization

$$p_n=\frac{N_n(m=+\frac{1}{2})-N_n(m=-\frac{1}{2})}{N_n(m=+\frac{1}{2})+N_n(m=-\frac{1}{2})}, \tag{2}$$

where $N_n(m)$ is the total number of protons with spin projection quantum number m. The Yb spins also have a highly anisotropic spin-lattice relaxation time $T_{1e}\propto[\cos^2\theta\sin^2\theta]^{-1}$, which has a minimum at $\theta=45°$ with a typical value 1 msec, but which becomes very long near $\theta=0°$ and 90°. A refrigerator cycle consists of the field pulse, and then the time elapsed when it is off. In the first part of a typical cycle, the pulsed field is turned on, $H_p\approx H_{dc}\sim15$ kOe, so that $H\sim21$ kOe and $\theta=45°$, so that T_{1e} is a minimum. The Yb spins rapidly reach thermal equilibrium described by the Boltzman distribution as shown in Fig. 2(a). The Yb spin polarization becomes $P_e=\tanh\Delta/2$, where $\Delta=g(\theta)\mu_BH/kT$; for $\theta=45°$, $H=21$ kOe, $T=1.2°$K, we find $\Delta=2.8$, so that $P_e=0.9$. In the second part of a cycle, the pulsed field is turned off rapidly compared to T_{1e}, but slowly compared to the Larmor precession period, i.e., adiabatically in the Ehrenfest sense, so the Yb spin-level populations remain unchanged, but the Yb energy-level separation becomes smaller at $\theta\to90°$, as shown in Fig. 2(b). If $g_\perp$ is small enough, at some angle near $\theta=90°$, $g(\theta)\approx g_n$, and energy-conserving mutual spin flips become energetically possible, as shown in Figs. 2(b) and 2(c); i.e., the Yb spin system and proton spin system approach a common spin temperature[9] by cross-relaxation.[10–13] After sufficiently many cycles, at least N_n/N_e, the protons should acquire the Yb spin polarization $P_e\sim0.9$, a value much larger than their own thermal equilibrium polarization $p_{n0}=\tanh(g_n\mu_BH_{dc}/2kT)\sim0.0013$, corresponding to an enhancement of p_n by a factor of 700.

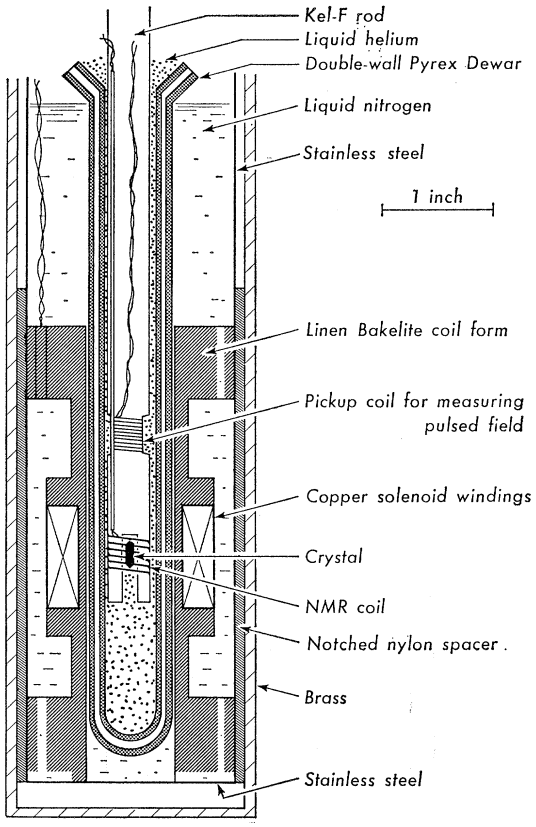

FIG. 3. Experimental apparatus for pulsed-field spin refrigerator.

Other types of spin refrigerator can be considered: The required cyclic Yb energy-level changes can be accomplished simply by rotating the crystal at a uniform speed. This was actually the first type of spin refrigerator to be considered. Robinson[14] first obtained proton polarization enhancements of ~10 in crystals of 1% Ce doped into $La_2Mg_3(NO_3)_{12}\cdot24H_2O$ (abbreviated as LMN). This material actually has $g_{11}\approx0$ rather than $g_\perp\approx0$ as in Yb:YES. Later, LJ obtained proton polarization of 19% in ^{172}Yb:YES by sample rotation at 60 rps in 10 kOe at 1.2°K. Their theoretical and experimental work indicated both that ^{172}Yb:YES is a favorable material for a spin refrigerator, and that higher operating speeds would increase the proton polarization obtained. To this end, we have constructed

[8] A. H. Cooke, F. R. McKim, H. Meyer, and W. P. Wolf, Phil. Mag. 2, 928 (1957).

[9] A Abragam and W. G. Proctor, Phys. Rev. 109, 1441 (1958).
[10] R. T. Schumacher, Phys. Rev. 112, 837 (1958).
[11] N. Bloembergen, S. Shapiro, P. S. Pershan, and J. O. Artman, Phys. Rev. 114, 445 (1959).
[12] P. S. Pershan, Phys. Rev. 117, 109 (1960).
[13] W. B. Mims and J. D. McGee, Phys. Rev. 119, 1233 (1960).
[14] F. N. H. Robinson, Phys. Letters 4, 180 (1963).

a pulsed field apparatus (similar to Fig. 1) capable of rotating the field, rather than the crystal, at 2 kc/sec. The highest proton polarization reported here is $p_n = 35\%$, obtained using this apparatus at $H_{dc} = 15.3$ kOe, $H_p = 20$ kOe, $T = 1.2°$K, and pulse repetition rate 20 pps.

Other nuclei can be polarized using the spin refrigerator effect.[15] Most notably, Lubbers and Huiskamp[16] obtained 97% polarization of radioactive ^{154}Mn in 0.1% Ce:LMN at $T = 0.2°$K by sample rotation.

In Sec. II, we describe the apparatus and materials we have used. In Sec. III we discuss the properties of Yb in YES. We present the essential features of nuclear spin-lattice relaxation in Sec. IV, as a preliminary to the theory of the spin refrigerator presented in Sec. V. Finally, we present results of both pulsed-field and rotating-crystal-spin refrigerator experiments in Sec. VI. Some of this work has been briefly reported earlier.[17,18]

II. APPARATUS AND MATERIALS

The pulsed field apparatus is shown in Fig. 3. Crystals are mounted in a Kel-F[19] holder in a double-wall Pyrex liquid ^{4}He Dewar. The 11 mm×18 mm Dewar tip is unsilvered to prevent eddy current heating. The pulsed-field solenoid, cooled by the LN bath, is constructed of 270 turns of #22 A.W.G. Teflon insulated copper magnet wire, wound on a linen Bakelite former. The windings have dimensions 22 mm i.d.×38 mm o.d.×24 mm long. The solenoid has inductance $L = 1510\,\mu H$ and resistance $R = 0.23\,\Omega$ at 77°K. The layers are insulated with etched Teflon tape and coated while winding with Shell Epon 828 Epoxy resin, mixed 10:1 with curing agent *D*. The inner jacket of the LN Dewar is thin-wall stainless steel to minimize eddy current heating.

Two different circuits are used to produce field pulses. The circuit of Fig. 4 produces roughly a half-sine pulse. A 3.5-μF capacitor bank is charged to $\sim$5 kV by R–C charging, then discharged through the solenoid by a type 5C22 hydrogen thyratron. When current reaches its maximum value, the voltage across the solenoid reverses, turning on a type 872 Hg vapor rectifier so that the energy stored in the magnetic field pulse is dumped into an $R \sim 15\,\Omega$ resistor. The value of R is chosen so that the *RLC* parallel circuit is somewhat underdamped, so that the pulse is turned off completely in a short time, but only a small back emf is developed across the thyratron, to prevent damage to it. A typical field pulse is shown in Fig. 5(a), which is the electronically integrated output from a small pickup coil wound just above the sample and lowered into position for measurements of H_p.

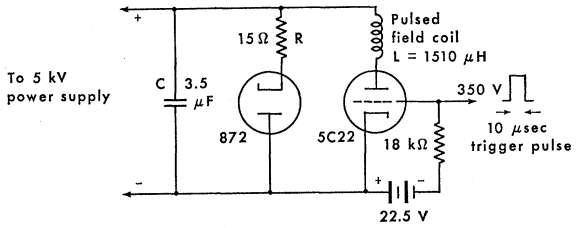

FIG. 4. Circuit for creating half-sine pulsed magnetic field.

A second circuit shown in Fig. 6 is used to produce roughly trapezoidal pulses. An 8.75-μF capacitor bank is charged by dc resonant charging,[20] then discharged into a 13.1-Ω resistor through a pulse-forming network[20] of which the pulsed-field solenoid is a part. Figures 5(b) and 5(c) show the current and field pulses produced, respectively. The difference between the current and field pulses is attributed to mutual inductive coupling between the solenoid and the brass LN Dewar outer jacket. We especially point out that the field is not turned off as soon as the current, but an exponentially decaying tail remains with a field of about 10% of the maximum pulsed field and decay time $\tau_0 = 275\,\mu$sec. In most of our experiments, the crystals were oriented so that Yb-proton cross-relaxation occurs during this tail of the pulse.

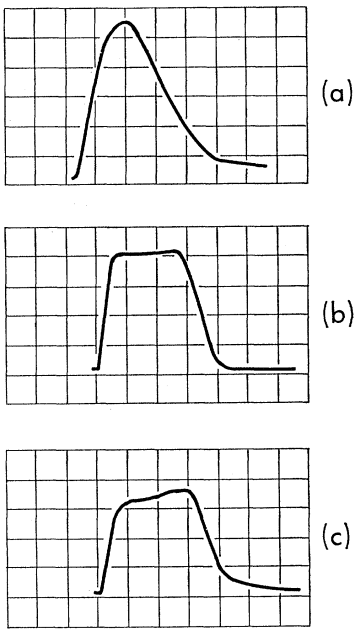

FIG. 5. (a) Oscillogram of half-sine pulsed field; time base: 50 μsec/div. (b) Trapezoidal pulsed current; time base: 100 μsec/div. (c) Trapezoidal pulsed field; time base: 100 μsec/div.

[15] W. G. Clark, G. Feher, and M. Weger, Bull. Am. Phys. Soc. **8**, 468 (1963).
[16] J. Lubbers and W. J. Huiskamp, Physica **34**, 193 (1967).
[17] J. R. McColl and C. D. Jeffries, Phys. Rev. Letters **16**, 316 (1966).
[18] J. R. McColl and C. D. Jeffries, Bull. Am. Phys. Soc. **11**, 906 (1966).
[19] Kel-F is the 3M Corporation trademark for poly-chlorotrifluoroethylene (PCTFE), a useful plastic containing no hydrogen PCTFE grease, useful for cementing samples in place is available from the Halocarbon Products Co., Hackensack, N. J.
[20] H. J. White, P. R. Gillette, and J. V. Lebacqz, in *Pulse Generators*, edited by G. N. Glasol and J. V. Labacqz (McGraw-Hill Book Co., New York, 1948), Chap. 6.

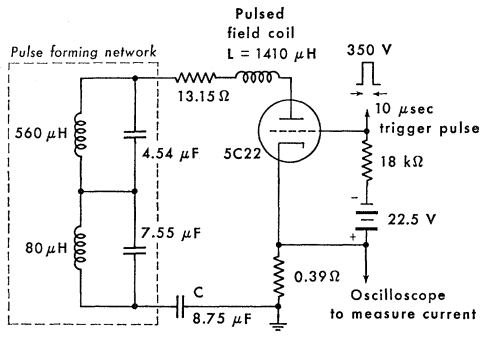

FIG. 6. Circuit for producing trapezoidal pulsed field.

During runs in which the trapezoidal pulse shape was used, samples were mounted in a sample holder which has an extra degree of freedom in that crystals can be rotated about a horizontal axis by a rack and pinion gear arrangement.

We also carried out rotating crystal experiments using LJ's apparatus, described in their paper.[2] This apparatus can mechanically rotate crystals at frequencies up to 60 rps in fields up to 22 kOe in temperatures down to 1.2°K. Shaft vibrations prevent this mechanical system from operating at the high switching speeds of the pulsed-field apparatus, however.

The proton NMR absorption signals were observed with a Q-meter circuit previously described.[21] We usually employed 60-cps field modulation and measured the peak height of the NMR absorption signal displayed on an oscilloscope. We often checked our measurements by also measuring the peak-to-peak first derivative signal obtained using 400-cps field modulation with lock-in detection. The two methods always agreed to within 3%, indicating that no important line-shape changes had occurred; significant NMR line-shape changes do occur in LMN crystals at high proton polarization.[22] All materials in the sample holder are hydrogen-free to prevent spurious proton NMR signals.

TABLE I. Crystals.

Crystal or sample number	Concentration of paramagnetic ion in growing solution	Host material	Chemical source Ion	Host
14	2% Yb^{172}	YES	a	b
16	0.7% Yb^{172}	YES	a	b
17	1% Yb^{172}	deuterated YES	a	b,c
18	2% Yb^{172}	YES	a	b
19	0.7% Yb^{172}	YES	a	b
20	0.7% Yb^{172}	YES	a	b

[a] Yb_2O_3: Oak Ridge National Laboratory, Series KJ, Sample 1245 A; enriched to 97.1% Yb^{172} isotope.
[b] $Y_2(SO_4)_3 \cdot 8H_2O$: Lindsay Chemical Co., Code 1148; Y~99.9999%.
[c] D_2O: General Dynamics Corporation, Batch XXVI, D_2O~99.7%.

[21] P. L. Scott, Thesis, University of California at Berkeley, 1961 (unpublished).
[22] T. J. Schmugge and C. D. Jeffries, Phys. Rev. **138**, A1785 (1965).

The crystals and chemicals used in their preparation are listed in Table I. Most of the crystals used were grown with Yb enriched to 97% isotopic abundance in ^{172}Yb. The Yb concentrations listed are the concentrations in the growing solution. A crystal from the same batch as crystals 14 and 18, which contained 2% ^{172}Yb in the growing solution, was found by optical absorption measurements to contain 0.6% Yb. Assuming the same rejection ratio, we calculate that the crystals grown from 0.7% Yb solution actually have 0.21% concentration.

The crystals could usually be adequately oriented with a polariscope but occasionally Laue x-ray scattering was used.

III. PROPERTIES OF Yb:YES

A. Crystal Structure of YES

The crystal structure of YES has been determined by Ketelaar[23] and refined by Fitzwater and Rundle.[24] The crystal space group is $P6_3/m$ (C_{6h}^2).[25] There are two magnetically equivalent Y sites per unit cell. The Y-site symmetry is C_{3h}. The H positions have not been determined by x-ray diffraction, but there is no evidence that the hydrogens lower the Y-site symmetry. We have estimated the H positions with these assumptions: the hydrogens also belong to $P6_3/m$ space group; the water molecules and ethyl radicals have the same dimensions as the free molecules; the water-molecule electric-dipole moments point toward Y sites; hydrogen-bond energies are minimized. We list these estimated positions in Table II along with the Y positions. Positions of the other heavy atoms are given in Ref. 24.

Figure 7 is a projection of all the atoms in a unit cell onto the $Z=\frac{1}{4}$ mirror plane; dashed lines denote hydrogen bonds. The figure and Table II suggest this set of nearest proton neighbors to the Y sites: (1) 12 protons belonging to set 7 waters at 3.04 Å; (2) 6 protons belonging to set 6 waters at 3.20 Å; (3) 6 protons belonging to set 9 carbons at 4.34 Å.

B. Paramagnetic Properties of Yb:YES

The Yb^{3+} ion has $4f^{13}$ ground configuration leading to $^2F_{7/2}$ and $^2F_{5/2}$ manifolds split about 10^4 cm^{-1} by spin-orbit coupling. Far-infrared spectroscopic absorption studies by Wheeler *et al.*[26] show that the ground state of Yb in YbES is the Kramers doublet $^2F_{7/2}$, $M_J=\pm\frac{3}{2}$, and that the first excited state at 44 cm^{-1} is a doublet mainly made up of $M_J=\pm\frac{5}{2}$ with some admixture of $M_J=\mp\frac{7}{2}$. We assume these results hold also for Yb in YES. The energy levels and wave functions that LJ determined by a crystal-field-parameter

[23] J. A. A. Ketelaar, Physica **4**, 619 (1937).
[24] D. R. Fitzwater and R. L. Rundle, Z. Krist. **112**, 362 (1959).
[25] *International Tables for X-Ray Crystallography*, edited by N. F. M. Henry and K. Lonsdale (Kynoch Press, Birmingham, England, 1952), Vol. I, p. 283.
[26] R. G. Wheeler, F. M. Reames, and E. J. Watchel, J. Appl. Phys. **39**, 915 (1968).

extrapolation procedure are very close to the results of Wheeler *et al.*, so we use LJ's calculations based on these wavefunctions, which we summarize below. At liquid-helium temperatures, only the ground doublet is significantly populated. We are interested mainly in the g values and spin-lattice relaxation rates of this doublet.

Spin-lattice relaxation. According to Van Vleck's[27] theory as modified by Orbach,[28] the paramagnetic spin-lattice relaxation rate of single ions is the sum of the rates of three processes:

$$T_{1e}^{-1}=T_D^{-1}+T_R^{-1}+T_0^{-1}, \quad (3)$$

where the three terms are the direct, Raman, and Orbach processes, respectively. The Raman and Orbach processes are two-phonon processes and have characteristic temperature dependences $T_R^{-1}=CT^9$ and $T_0^{-1}=Be^{-\Delta/KT}$, where $\Delta=44$ cm^{-1} is the energy of the first excited doublet. Using Scott and Jeffries's[29] version of Orbach's method, LJ calculate $C=1.7\times10^{-2}$ sec^{-1} °K^{-9} and $B=3.5\times10^{11}$ sec^{-1}. Their estimates agree substantially with $C=1.55\times10^{-2}$ and $B=7\times10^{11}$ measured in YbES by Van den Broek and Van der Marel.[30] Below 2.5°K the Raman process strongly dominates the Orbach process. LJ use their proton spin lattice relaxation data to determine $B=7\times10^{11}$ sec^{-1} and $C=8\times10^{-2}$ sec^{-1} °K^{-9}, which we take to be the most accurate experimental values for Yb in YES.

The direct process arises from absorption or emission of a single phonon; this has unfortunately not yet been measured for Yb:YES. However, LJ also used the Scott-Jeffries[29] procedure to estimate

$$T_D^{-1}=A'H^5\sin^2\theta\cos^3\theta\coth[g_{\parallel}\mu_BH\cos\theta/2kT], \quad (4)$$

with $A'=1.38\times10^{-16}$ sec^{-1} Oe^{-5}. For $g_{\parallel}\mu_BH\cos\theta<2kT$, Eq. (4) simplifies to

$$T_D^{-1}\approx AH^4T\cos^2\theta\sin^2\theta, \quad (5)$$

with $A=1.2\times10^{-12}$ sec^{-1}Oe^{-4}, which we use, for simplicity, in the following calculations. LJ's proton spin-lattice relaxation time measurements led them to conclude that A' is approximately 5 times lower than their estimate above.

g values. For the lowest doublet given by Wheeler *et al.*,[26] the calculated g values are given by Eq. (1) with $g_{\parallel}=3.43$ and $g_{\perp}=0$. Cooke *et al.*,[8] and Van den Broek and Van der Marel[30] have measured $g_{\parallel}=3.40\pm0.07$, $g_{\perp}=0\pm0.05$ in YbES by magnetic susceptibility measurements. Schmugge has measured $g_{\parallel}=3.37\pm0.07$, $g_{\perp}<0.5$ in 5% Yb:LaES, by electron spin resonance.

It is unfortunate that $g_{\perp}$ is not better known, because knowledge of it is important in understanding Yb-proton cross-relaxation. For example, if $g_{\perp}=0$ exactly,

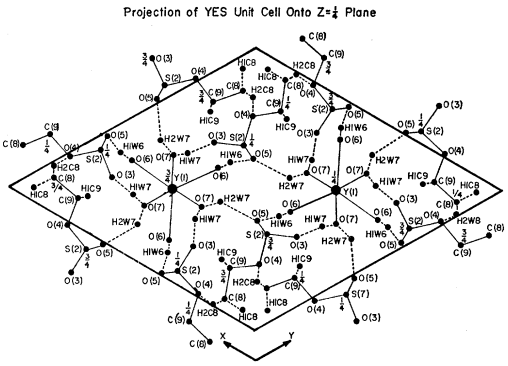

FIG. 7. Projection of YES unit cell onto $Z=\frac{1}{4}$ mirror plane. The positions of heavy atoms are from Ref. 24; of protons, from Sec. III. Dashed lines show hydrogen bonds.

there does exist an angle θ such that $g(\theta)=g_n$ so that cross-relaxation is energetically allowed, but the matrix elements for the process vanish. This can be seen from the form of the Yb-proton dipole-dipole Hamiltonian, Eq. (B3) in Appendix B; the amplitude of the $S_+{}^iI_+{}^j$ perturbation which gives mutual spin flips is proportional to $g_{\perp}$. Physically, a spin needs a "handle" on it to be flipped. Conversely, if $g_{\perp}>g_n$, then $g(\theta)>g_n$ for all θ, and cross-relaxation processes involving one proton and one Yb are energetically forbidden. Thus, knowledge of $g_{\perp}$ is important even in understanding which cross-relaxation processes are allowed, as well as in calculating the magnitude of the effect. Since no experiments have yielded precise enough values of $g_{\perp}$, we must consider theoretically all mechanisms which can contribute to $g_{\perp}$. We first mention that $g_{\perp}=0$, calculated from Wheeler's wave functions, is due to the purity of the wavefunctions, which is a result of C_{3h} symmetry. It is therefore evident that only new interactions which destroy the C_{3h} symmetry can cause $g_{\perp}\neq0$.

C. Hyperfine Interactions

For ^{171}Yb and ^{173}Yb, the existence of nuclear spin produces energy levels of the Yb electronic spin which are determined by an effective local field $\mathbf{H}_{\rm loc}=\mathbf{H}+\mathbf{H}_{\rm hyp}$, where $\mathbf{H}$ is the external field and $\mathbf{H}_{\rm hyp}$ is the hyperfine field exerted by the Yb nucleus on the Yb electrons. In

TABLE II. Positions of atoms in yttrium ethyl sulfate: space group[a]: $P6_3/m$. $a=13.924$ Å, $c=7.057$ Å.

Set[a]	Atom	x	y	z	Ref.
2(c)	Y(1)	0.3333	0.6667	0.2500	b
12(i)	H1W6	0.3550	0.4551	0.3575	c
12(i)	H1W7	0.2228	0.4973	0.5763	c
12(i)	H2W7	0.1396	0.5285	0.5137	c
6(h)	H1C8	0.0994	0.0532	0.7500	c
12(i)	H2C8	0.1815	0.0094	0.8761	c
12(i)	H1C9	0.3157	0.1832	0.8761	c

[a] Reference 25. [b] Reference 24. [c] Section III A.

[27] J.H. Van Vleck, Phys. Rev. **57**, 426 (1940).
[28] R. Orbach, Proc. Roy. Soc. (London) **A264**, 458 (1961); **A264**, 485 (1961).
[29] P. L. Scott and C. D. Jeffries, Phys. Rev. **127**, 32 (1962).
[30] J. Van den Broek and L. C. Van der Marel, Physica **30**, 565 (1964).

our experiments, we rotate $\mathbf{H}$ continuously through the $\theta=90°$ plane, so $\mathbf{H}_{\rm loc}$ also passes through this plane, but slightly earlier or later than the time when $\mathbf{H}$ is in this plane. Thus, there is an apparent macroscopic broadening of the cross-relaxation processes, but there is no effect microscopically.

D. Pair Interactions

Even in dilute crystals, Yb^{3+} ions experience nonnegligible interaction with other Yb^{3+} ions. For example, in a 0.6% Yb:YES crystal, about 5% of the Yb^{3+} ions have other Yb^{3+} ions as nearest neighbors. Nevertheless, pair interactions will be unimportant, because by far the dominant pair interaction is the magnetic dipole-dipole interaction which effectively only changes the local field at each Yb side; the effect is similar to the hyperfine interaction.

E. Third-Order Zeeman Splitting

The Zeeman interaction admixes excited crystal field doublets to the ground doublet producing a ground doublet splitting proportional to H^3. LJ calculated $g_\perp=3.2\times10^{-12}H^2$ so that $g_\perp=g_n$ at $H=30\,000$ Oe, showing that the third-order Zeeman splitting is extremely small in YbES, and we neglect it.

F. Dynamic Crystal-Field Distortions

Several authors[31,32] have recently pointed out that dynamic crystal-field distortions due to zero-point lattice motion produce sizeable g-shifts. Physically, this effect arises because the instantaneous crystal field always has lower symmetry than the time-average crystal field, because of zero-point lattice motion. However, it can be shown[33] that when any g factor vanishes because of symmetry, and further if the irreducible representations of the point symmetry group are all one dimensional (this is true of C_{3h}[34]), then that g factor will still vanish even in the presence of zero point lattice motion. Thus, this effect does not alter $g_\perp$ in YbES.

G. Static Crystal-Field Distortions

The above argument does not apply to static crystal-field distortions, due to lattice vacancies, interstitial atoms, impurities, dislocations, external stress, stacking faults, etc., which may lower the symmetry at a given Yb site. Since this is the only mechanism that can produce sizeable deviations of $g_\perp$ from zero, we consider this effect in detail.

If $\mathcal{H}_S$ is the part of the crystal-field Hamiltonian due to static strain, then the zero-order crystal-field ground doublet wave functions $|\pm a\rangle^0$ are changed in first order to

$$|\pm a\rangle=|\pm a\rangle^0-\sum_{\pm e}\frac{|\pm e\rangle^0\,{}^0\langle\pm e|\mathcal{H}_S|\pm a\rangle^0}{E_e}, \quad (6)$$

where $|\pm e\rangle^0$ and E_e denote all the excited-state wave functions and energies. By definition, $g_\perp$ is given by

$$g_\perp=g_L|\langle+a|J_++J_-|-a\rangle|, \quad (7)$$

where g_L is the Lande g factor. This is generally nonzero even if ${}^0\langle+a|J_++J_-|-a\rangle^0=0$. A first-principles calculation of $g_\perp$ is impossible since $\mathcal{H}_S$ and even the dominant effect contributing to $\mathcal{H}_S$ are unknown. Furthermore, it is evident, since $\mathcal{H}_S$ varies from site to site, that there exists not a unique value of $g_\perp$ in YbES but a distribution of values. Therefore, we must make a reasonable guess at the form and width of $\rho(g_\perp)dg_\perp\equiv$ the fraction of ions that have $g_\perp$ between $g_\perp$ and $g_\perp+dg_\perp$.

As a start, consider the form of $\mathcal{H}_S$ appropriate to cubic crystals, given by Feher.[35] We find that longitudinal strains produce real matrix elements ${}^0\langle\pm e|\mathcal{H}_S|\pm a\rangle^0$ while shear strains produce imaginary matrix elements. The Hamiltonian is more complicated in hexagonal crystals such as YbES, but indeed we expect both real and imaginary contributions to the matrix element in Eq. (7), so that upon squaring this equation we will have two independent contributions to $g_\perp^2$:

$$g_\perp^2=(g_\perp^2)_{\rm real}+(g_\perp^2)_{\rm imag}. \quad (8)$$

The actual values of $(g_\perp)_{\rm real}$ and $(g_\perp)_{\rm imag}$ will be proportional to certain components of $\mathcal{H}_S$. Finally, we note that in experimental studies[35,36] of EPR lines sensitive to strain, the observed EPR line shapes were Lorentzian. We therefore assume that $(g_\perp)_{\rm real}$ and $(g_\perp)_{\rm imag}$ each have Lorentzian distributions of, say, equal width, so that the over-all distribution is a folding of two Lorentzian line shapes:

$$\rho(g_\perp)=\frac{2\sqrt{2}g_0}{\pi}\frac{1}{g_0^2+g_\perp^2}\left[\frac{g_\perp^2}{\frac{1}{2}g_0^2+g_\perp^2}\right]^{1/2}, \quad (9)$$

where g_0^2 is the second moment of the distribution. Figure 8 shows the assumed distribution. We estimate g_0 by assuming that observed linewidths in all the dilute rare-earth ethyl sulfates are due to random static strains. These linewidths are typically 3 to 20 Oe in several thousand Oe, so that we estimate $g_0\approx0.003$ to 0.02. In Sec. VI A it turns out that choosing $g_0\approx0.003\approx g_n$ gives a best fit with spin refrigerator polarization data.

The question of whether g_0 varies from crystal to crystal is difficult. The internal strains are probably due to dislocations[36,37] and/or stacking faults and so may depend on sample preparation and handling, but not

[31] M. Inoue, Phys. Rev. Letters **11**, 196 (1963).
[32] R. J. Birgeneau, Phys. Rev. Letters **19**, 160 (1967).
[33] We are indebted to R. J. Birgeneau and R. Orbach for bringing the result to our attention.
[34] J. C. Prather, *Atomic Energy Levels in Crystals* (National Bureau of Standards Monograph No. 19, U. S. Government Printing Office, Washington, D. C., 1961).
[35] E. Feher, Phys. Rev. **136**, A145 (1964).
[36] D. H. McMahon, Phys. Rev. **134**, A128 (1964).
[37] A. M. Stoneham, Proc. Phys. Soc. (London) **89**, 909 (1966); J. Phys. C. **1**, 565 (1968).

much on sample purity. All our crystals were grown under the same conditions from the same chemicals, but polycrystalline samples were ground to a powder from single crystals. One would think this can introduce dislocations, but nevertheless the same value of g_0 gives good predictions of proton polarization results for both single and polycrystalline samples.

IV. PROTON SPIN-LATTICE RELAXATION IN Yb:YES

Although we present no new results on proton spin-lattice relaxation in this paper, we review the features of the theory that are useful in developing the theory of the spin refrigerator in Sec. V. In a pioneering work, Bloembergen[38] showed that nuclei in very dilute paramagnetic insulators relax to the lattice temperature by a combination of two effects: direct relaxation to paramagnetic impurities via modulation of the impurity magnetic dipole field, as the impurity relaxes to the lattice; and nuclear spin diffusion, i.e., cross-relaxation between nuclear spins. We are especially interested in exploiting the properties of nuclear spin diffusion, which carries the enhanced proton polarization away from the immediate vicinity of the Yb spins to the distant protons.

A simplified diffusion equation for proton polarization can be written down provided one assumes that the nuclear polarization $p_n{}^j$ of the jth site does not vary much from site to site, so it can be approximated by a continuous function of position $p_n(\mathbf{r}_j)$. Actually, a given proton spin is either up or down; $p_n{}^j$ is an *ensemble* average over a large number of identical crystals. The diffusion equation is[38]

$$\frac{\partial p_n(\mathbf{r}_j,t)}{\partial t}=\nabla\cdot[D\nabla p_n(\mathbf{r}_j,t)]+\sum_i \frac{C}{|\mathbf{r}_j-\mathbf{r}_i|^6}[p_{n0}-p_n(\mathbf{r}_j,t)]. \quad (10)$$

The first term on the right-hand side is the spin-diffusion term, where the diffusion coefficient may have a typical value $D\approx 10^{-12}$ cm^2/sec, and which may depend on position. The second term is the sum of direct spin-lattice relaxation terms from each paramagnetic impurity at r_i. Bloembergen's expression for the coefficient C (not to be confused with the Raman coefficient; this notation is used for historical reasons) is modified for Yb in YES because of the anisotropy of the Yb g factor. If we assume that the complicated angular dependence of C can be averaged out, it can be shown[39] that

$$C=\frac{3}{10}\left(\frac{g_D\mu_B}{H}\right)^2\frac{\tau_c^{-1}}{1+(\omega_n\tau_c)^{-2}}\operatorname{sech}^2\left(\frac{\hbar\omega_e}{2kT}\right), \quad (11)$$

[38] N. Bloembergen, Physica **15**, 386 (1949).
[39] J. R. McColl, Thesis, University of California at Berkeley, 1967 (unpublished).

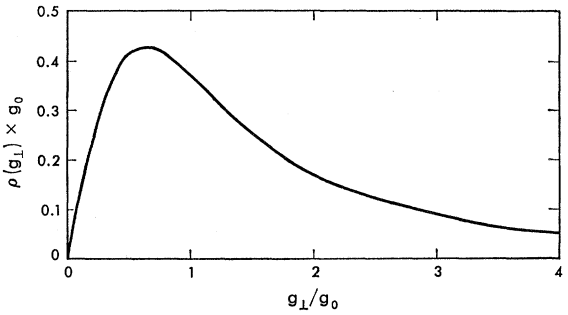

FIG. 8. Distribution of $g_\perp$-values assumed for Yb in YES. The curve is Eq. (9).

where, in general,

$$\frac{3g_D{}^2}{10}=\frac{3}{10}g^2(\theta)+\frac{7}{20}\cos^2\theta\sin^2\theta\left[\frac{g_\perp{}^2-g_{11}{}^2}{g(\theta)}\right]^2, \quad (12)$$

which for $g_\perp=0$ becomes

$$\frac{3}{10}g_D{}^2=\frac{6+\sin^2\theta}{20}g_{11}{}^2\simeq\frac{3}{10}g_{11}{}^2. \quad (13)$$

In Eq. (11) ω_e and ω_n are the Yb and proton Larmor precession frequencies, respectively. The Yb spin correlation time τ_c we take to be T_{1e}. Furthermore, for the range of fields and temperatures of interest, $\omega_n T_{1e}\gg 1$, so that

$$C\approx\frac{3}{10}\left(\frac{g_{11}\mu_B}{H}\right)^2\frac{1}{T_{1e}}\operatorname{sech}^2\left(\frac{\hbar\omega_e}{2kT}\right). \quad (14)$$

Several authors[40–44] have constructed approximate analytic solutions to Eq. (10). These solutions involve rather complicated combinations of Bessel functions of fractional order. Goldman[45] has pointed out a simple, physically intuitive alternate way to arrive at the same result; we shall adopt and generalize his approach. We divide the crystal into spheres of influence,[7,22] each having a Yb spin at its center. Each sphere has radius $R=(3/N4\pi)^{1/3}$, where N is the Yb density per cm^3, so that N of these spheres occupy 1 cm^3. A characteristic length occurring in the solution of Eq. (10) is $b=0.68\,[C/D]^{1/4}$, called the scattering radius by de Gennes.[42] The physical significance of b is that, neglecting static dipolar fields, protons inside a subshell of radius b relax faster by direct relaxation than by spin diffusion (hence, rapidly and nonexponentially). Protons outside b but inside R relax faster by spin diffusion. For low Yb concentrations, $b\ll R$, so these protons are in the vast

[40] G. R. Khutsishvili, Phys. Inst. Georgia Acad. Sci. **2**, 115 (1954); **4**, 3 (1956).
[41] G. R. Khutsishvili, Zh. Eksperim. i Teor. Fiz. **42**, 1311 (1962) [English transl.: Soviet Phys.—JETP **15**, 909 (1962)].
[42] P. G. deGennes, J. Phys. Chem. Solids **3**, 345 (1958).
[43] W. E. Blumberg, Phys. Rev. **119**, 79 (1960).
[44] H. E. Rorschach, Jr., Physica **30**, 38 (1964).
[45] M. Goldman, Phys. Rev. **138**, A1675 (1965).

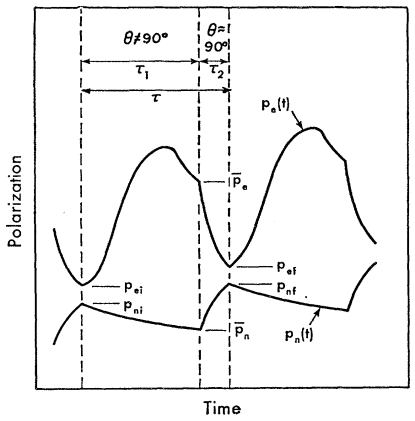

FIG. 9. Schematic illustration of Yb spin polarization p_e and proton polarization p_n for a typical spin-refrigerator cycle.

majority. These outer protons are in such strong thermal contact with each other that they essentially have a common polarization and relax together exponentially with a rate determined by their average direct relaxation rate

$$\frac{1}{T_{1n}}=\int_b^R d^3r\frac{C}{r^6}\Big/\int_b^R d^3r\simeq\frac{C}{b^3R^3}. \tag{15}$$

But the above treatment cannot be really correct, as pointed out by Bloembergen[38] and Blumberg,[43] for there exists another characteristic radius d called the diffusion barrier radius. Inside this diffusion barrier, the local static dipolar field of the Yb spin is strong enough to inhibit spin diffusion. Khutsishvili[41] estimates $d=a(3\mu_e/\mu_n)^{1/4}$, where μ_e and μ_n are the static Yb and proton magnetic moments, respectively, and a is the interproton spacing. For $a=1.6$ Å, the proton-proton distance in H_2O, we calculate $d=12.2$ Å for Yb:YES. These authors[38,41,42] assume $D=0$ for $r<d$. We think it is more realistic to assume a nonzero value $D(r<d)\ll D(r>d)$. The nuclear spin-lattice relaxation rate of Eq. (15) is still valid provided b is replaced by the solution to the transcendental equation

$$b=0.68[C/D(b)]^{1/4}. \tag{16}$$

If one assumes $D(r<R)=0$, then solutions to Eq. (16) always give $b\equiv d$ and $T_{1n}^{-1}\leqq C/(dR)^3$. This expression predicts relaxation rates two orders of magnitude slower than observed by LJ in Yb:YES as well as those observed by several workers in Nd-doped LMN.[22,46] These authors are able to fit their results very well by the expression, which they derived from elementary arguments,

$$1/T_{1n}=C/r_1^3R^3, \tag{17}$$

where r_1 is the distance from the impurity spin to its *nearest-neighbor* proton. Thus, we must clearly drop the assumption $D(r<b)=0$, since $b=r_1$ is implied by comparing Eqs. (15) and (17). This means that $D(r)$ is finite for all the protons in the crystal. Taking $C\leqq 3\times10^{-44}$ cm^6/sec as the largest value encountered in LJ's work, we estimate that $D(r_1)$ is at least as large as 10^{-14} cm^2/sec. This value of D seems unreasonably large since the Yb local field at $r_1\approx3.1$ Å is ≈1000 Oe compared to the proton linewidth, 15 Oe, observed in YES. Nevertheless, we are forced to accept this anomalously large value of D inside the diffusion barrier because of the goodness with which Eq. (17) fits so much T_{1n} data in YES and LMN.

We have also shown formally in a lengthy calculation[39] that solutions to Eq. (10) can be found assuming a usual value of D for $r>d$ and a much smaller but finite value for D for $r<d$. The results agree with Eq. (17).

Both the heuristic approach taken above and the more rigorous but lengthy calculation given elsewhere[39] give this most important result: When Eq. (17) holds experimentally, all the protons in the crystal, even those very near paramagnetic ions, have nearly the same polarization. We will use this result in solving the diffusion equation which applies during operation of a spin refrigerator.

V. THEORY OF SPIN REFRIGERATOR

The goal of this section is to write down and solve a diffusion equation for the proton spin polarization during the operation of a spin refrigerator. The problem is made enormously simpler because the anisotropic spin-lattice relaxation rate for both Yb spins and protons is nonzero only for $\theta\neq90°$, while Yb-proton cross-relaxation occurs only very near $\theta=90°$. Thus these two different relaxation mechanisms separate naturally, as shown in Fig. 9. In Sec. V A, we investigate the spin-lattice relaxation portion of a cycle, neglecting spin diffusion; in Sec. V B, the cross-relaxation portion; and in Sec. V C, we combine the results of Secs. V A and V B to formulate and solve a diffusion equation.

A. Spin-Lattice Relaxation Portion of a Cycle

During the lattice relaxation part of a cycle, i.e., time τ_1 in Fig. 9, the Yb and proton-spin polarizations

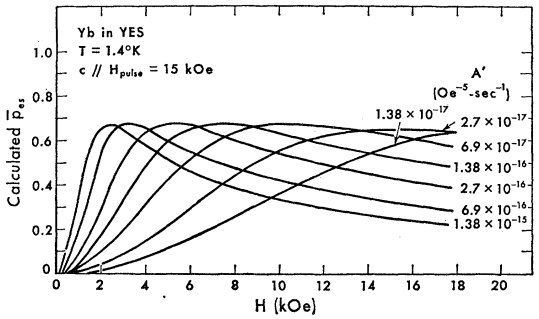

FIG. 10. Calculated values of $\bar{p}_{es}$ versus H_{dc} for "half-sine"–pulsed-field spin refrigerator of Fig. 5(a).

[46] T. E. Gunter and C. D. Jeffries, Phys. Rev. 159, 290 (1967).

(neglecting spin diffusion) independently obey the equations

$$\frac{dp_e}{dt}=\frac{1}{T_{1e}(t)}[p_{e0}(t)-p_e(t)], \tag{18a}$$

$$\frac{dp_n}{dt}=\frac{1}{T_{1n}(t)}[p_{n0}-p_n(t)]. \tag{18b}$$

Equation (18a) has a formal solution given by LJ:

$$\bar{p}_e-p_{ei}=K_e(\bar{p}_{es}-p_{ei}), \tag{19}$$

where p_{ei} is the polarization at the beginning of this part of the cycle, $\bar{p}_e$ is the polarization after τ_1, and

$$K_e=1-\exp\left[-\int_0^{\tau_1}T_{1e}^{-1}(t)dt\right], \tag{20}$$

is a measure of the completeness of lattice relaxation during a cycle. In the steady state after roughly $1/K_e$ cycles $\bar{p}_e$ builds up to $\bar{p}_{es}$,

$$\bar{p}_{es}=\frac{1-K_e}{K_e}\int_0^{\tau_1}\exp\left[\int_0^t T_{1e}^{-1}(t')dt'\right]\frac{p_{e0}(t)}{T_{1e}(t)}dt. \tag{21}$$

For a rotating crystal spin refrigerator at a frequency f_R, using T_{1e}^{-1} given by Eq. (5), we calculate the asymptotic solutions for the Yb polarization as $T\to\infty$, $f_R\to\infty$,

$$\bar{p}_{es}\sim(\bar{p}_{es})_\infty=\frac{32}{15\pi}\frac{g_{11}\mu_B H}{2kT}. \tag{22}$$

In the very low-frequency limit $f_R\to 0$, $T\to\infty$, we have

$$\bar{p}_{es}\sim(\bar{p}_{es})_0=\Gamma(\tfrac{4}{3})\left[\frac{6\pi f_R}{AH^4T}\right]^{1/3}\frac{g_{11}\mu_B H}{2kT}. \tag{23}$$

For intermediate rotation speeds and low temperatures, the expression

$$\bar{p}_{es}=\tanh\{[(\bar{p}_{es})_\infty^{-9}+(\bar{p}_{es})_0^{-9}]^{-1/9}\}, \tag{24}$$

agrees very well with exact numerical calculations performed by LJ.

For a pulsed-field spin refrigerator, no solution for $\bar{p}_{es}$ in terms of ordinary functions is possible because of the somewhat arbitrary shape of the field pulses. We have performed numerical integrations of Eq. (18a) for the Yb polarization, with the results displayed in Figs. 10 and 11, for half-sine and trapezoidal pulses, respectively. Since the direct process coefficient A' is not well known, we present a family of curves for various values of A'. The decrease in $\bar{p}_{es}$ at higher fields is due to the fact that T_{1e}^{-1} is becoming so great that the Yb spins relax back to the lower value of p_{e0} at the end of τ_1. The importance of $\bar{p}_{es}$ for both types of spin refrigerator is that in steady-state operation, the Yb spins have this polarization just before the cross-relaxation portion of a cycle. For the ideal case, the protons eventually acquire this polarization.

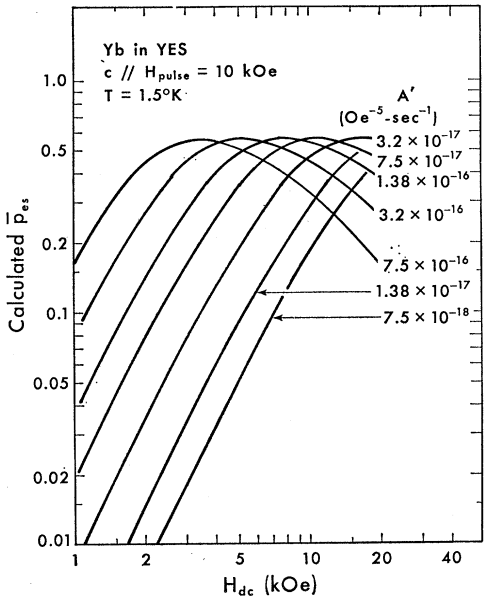

FIG. 11. Calculated values of $\bar{p}_{es}$ versus H_{dc} for "trapezoidal"-pulsed-field spin refrigerator of Fig. 5(c).

For spin refrigerators operated at reasonable speeds, $\tau_1\ll T_{1n}$, so that the change in proton polarization in this part of the cycle (neglecting spin diffusion) is just

$$\bar{p}_n{}^j-p_{ni}{}^j=\sum_i\frac{\langle C\rangle\tau_1}{|\mathbf{r}_i-\mathbf{r}_j|^6}(p_{n0}-p_{ni}{}^j), \tag{25}$$

where $\langle C\rangle$ is the average of C in Eq. (14) over the refrigerator cycle, and $p_{n0}=\tanh(g_n\mu_B H/2kT)$ is the thermal equilibrium proton spin polarization.

B. Cross-Relaxation Part of a Cycle

Previous treatments of cross-relaxation[9–13] have analyzed spin systems in which the cross-relaxation time T_{12} is much longer than the internal equilibrium time of an individual spin system. This means that each spin system forms a thermal reservoir with unique spin temperature during the cross-relaxation process. This treatment cannot be validly applied to Yb-proton cross-relaxation for a number of reasons: Each Yb spin has $g_\perp$ differing from every other Yb spin, implying that each Yb spin has different cross-relaxation transition probabilities from other Yb spins. The protons forming the proton spin system vastly outnumber the Yb spins; for 0.6% Yb: YES, there are 5500 protons in a sphere of influence, each having a unique site in the sphere and

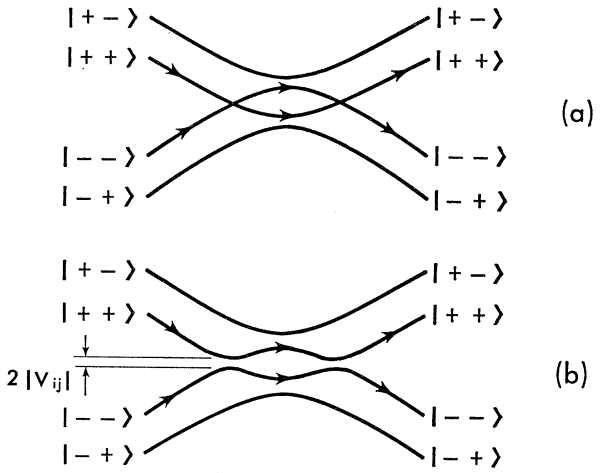

FIG. 12. Coupled energy levels of Yb spin and a typical proton. (a) $|V_{ij}|<\delta E$ (proton linewidth) so $|-\ -\rangle$ level crosses $|+\ +\rangle$ level and cross-relaxation occurs. (b) $|V_{ij}|>\delta E$ so that adiabatic passage path is followed and no cross-relaxation occurs.

hence a unique set of cross-relaxation transition probabilities. Finally, although it is true that $T_{12}>T_{2n}\sim 10^{-5}$ sec (T_{2n} is the proton spin-spin equilibrium time), T_{12} plays the role of a *local* equilibrium time. The *bulk* equilibrium time is of the order of the diffusion time between Yb sites, $4R^2/D\sim 0.3$ sec, much longer than T_{12} or T_{2n}. Therefore we use a new approach to cross-relaxation, finding the effect of this part of a refrigerator cycle on individual spins. This result is combined with the result of the previous section, i.e., we find the net change in individual spin polarization due to a whole refrigerator cycle. This is then to be inserted into a spin-diffusion equation which will then also take into account equilibrium processes within the proton spin system.

We first investigate the simplest cross-relaxation process in which one Yb spin and one proton simultaneously flip. The details are given in Appendix A, with the proton polarization at the end of a cross-relaxation cycle given by Eq. (A7).

Multiple spin flips. It is energetically favorable for m Yb spins to flip n protons if $m\Delta_e=n\Delta_n$. We consider only processes involving $m=1$ because the large Yb-Yb spacing in highly dilute crystals makes processes involving two or more Yb spins relatively unlikely. However, the processes in which $n=\epsilon=\Delta_e/\Delta_n$ protons flip can be quite frequent. They are important because the Yb spin temperature at the beginning of cross-relaxation is $T_S\approx\Delta_e/(k\bar{p}_{es})\propto\epsilon$. In multiple spin-flip cross-relaxation, protons and Yb spins approach a common spin temperature, rather than polarization, so that the larger ϵ is, the higher the spin temperature that protons will reach; hence they become less highly polarized. This effect is treated quantitatively in Appendix B. The conclusion is that at high fields and fast rotation, 1:1 flips dominate, but at lower fields and frequencies, 1:1, 2:1, and 3:1 flips all contribute.

Adiabatic passage corrections. When the spin-flip part of the Yb-proton dipolar interaction exceeds the proton linewidth, then time-dependent perturbation breaks down. Figure 12 shows the coupled energy levels of a Yb spin and a typical proton in the neighborhood of $\theta=90°$. In Fig. 12(a), $|V_{ij}|<\delta E$, the proton linewidth, so the levels actually cross, and we can use perturbation theory as above. However, in Fig. 12(b), in which $|V_{ij}|>\delta E$, the levels which crossed in (a) are now split by $2|V_{ij}|$, greater than the linewidth, so that they no longer cross, and $W_{ij}\to 0$. According to the Ehrenfest principle, the populations of the energy levels do not change if the external parameters are varied slowly enough; i.e., cross-relaxation does not occur. However, the Ehrenfest principle is not always obeyed; Wannier[47] has shown that the probability that the Ehrenfest principle is *obeyed* when two levels cross at rate $\dot{E}$, is $P=1-e^{-2\pi|V_{ij}|^2/\hbar\dot{E}}$. By comparison with Eqs. (A4) and (A6), this is exactly the probability for complete cross-relaxation (if there were only one proton). Therefore, if $|V_{ij}|^2\gg\hbar\dot{E}$, we would calculate $f_1=1$ implying complete cross-relaxation between the proton and Yb spin; but if $|V_{ij}|>\delta E$ also obtains, then $P=1$, which implies that the Ehrenfest principle is obeyed so that no cross-relaxation occurs. Thus completely misleading results are obtained if adiabatic passage effects are ignored.

Nevertheless, we now show that for the range of fields and rotation speeds of our experiments, no corrections are necessary. For the protons nearest to Yb sites, we calculate $|V_{ij}|=4.4\times10^{-21}$ erg. The observed proton NMR linewidth in YES is 14 Oe, so that $\delta E=3.9\times10^{-22}$ erg; we expect to have the use the adiabatic passage picture for the nearest protons. Nevertheless, if we exclude all protons for which $|V_{ij}|>\delta E$ in the sum of Eq. (A4), we still get $\sum_j|V_{ij}|^2=1.2\times10^{-41}\text{erg}^2$, which yields nearly complete cross-relaxation for our experimental conditions. This means that even though the near neighbor protons are prevented from taking part in 1:1 cross-relaxation, enough farther neighbors take part in the process so that it remains complete; i.e., the Yb spin is always flipped. Equation (B5a) is corrected by the new expression $f_1=1-e^{-1.15\times10^{-14}/\dot{E}}$. Our highest field $H=20\,000$ Oe and rotation speed $f_R=60$ rps are actually just at the borderline for validity of the above argument; for higher fields or rotation speeds, adiabatic passage effects will certainly have to be taken into account.

We find that no corrections are necessary for 2:1 and 3:1 spin flip processes.

C. Diffusion Equation for Spin Refrigerator

The net change in proton and Yb spin polarizations due to a whole refrigerator cycle can now be found from Eqs. (19), (25), (B1), and (B2). After roughly $1/K_e$ cycles, the Yb spin polarization reaches quasi-steady-state, and the change in proton polarization during an

[47] G. H. Wannier, Physics 1, 251 (1965).

entire cycle $\delta p_n{}^j = p_{nf}{}^j - p_{ni}{}^j$, is

$$\delta p_n{}^j = \sum_i \left(\frac{q_{ij}}{\sum_k q_{ik}} \left\{ \frac{K_e \langle \epsilon f_\epsilon \rangle_i \bar{p}_{es}}{1-(1-K_e)\langle 1-f_\epsilon \rangle_i} - \left[\langle \epsilon^2 f_\epsilon \rangle_i - \frac{(1-K_e)\langle \epsilon f_\epsilon \rangle_i{}^2}{1-(1-K_e)\langle 1-f_\epsilon \rangle_i} \right] \langle \bar{p}_n \rangle_i \right\} - \frac{\langle C \rangle \tau (\bar{p}_{ni}{}^j - p_{n0})}{r_{ij}{}^6} \right). \quad (26)$$

We emphasize that there are three different kinds of average brackets in Eq. (26): $\langle C \rangle$, from Eq. (25), represents a time average over a refrigerator cycle; $\langle p_n \rangle_i$, from Eqs. (A4) and (B1), is the average proton polarization about the ith Yb site weighted by $r_{ij}{}^{-6}$; and $\langle \epsilon f_\epsilon \rangle_i$, $\langle \epsilon^2 f_\epsilon \rangle_i$ and $\langle 1-f_\epsilon \rangle_i$ represent the net effect of all orders of cross-relaxation processes. The factor $1-(1-K_e)\langle 1-f_\epsilon \rangle$ which appears in the denominator in several places in Eq. (26) always turned out to be unity in our calculations, so we now drop it.

We derive a diffusion equation simply by adding $[\dot{p}_n(\mathbf{r}_j)]_{\text{spin refrigerator}} \approx \delta p_n{}^j/\tau$ to the diffusion term of Eq. (10):

$$\frac{\delta p_n(\mathbf{r}_j)}{\delta t} = \nabla \cdot D \nabla p_n(\mathbf{r}_j) + \frac{\delta p_n{}^j}{\tau}. \quad (27)$$

We wish ultimately to calculate the steady-state proton polarization p_{ss}, the average proton polarization which is obtained after operating a spin refrigerator for a long enough time that no further change occurs, i.e., $\sum_j \delta p_n{}^j = 0$. Our solution to the diffusion equation is guided by the discussion of spin-lattice relaxation in Sec. IV. In that section we pointed out that proton spin-lattice relaxation results in Yb:YES could be accounted for by assuming $b = r_1$; this implies $p_n(\mathbf{r})$ is sensibly uniform over the whole crystal. Now, since our observed polarization buildup times are all at least as long as 10 sec, which is also the shortest proton spin-lattice relaxation times that LJ fit to Eq. (17), and since both processes have a $r_{ij}{}^{-6}$ dependence through the Yb-proton dipole-dipole interaction, it is reasonable to assume that $p_n(\mathbf{r})$ is also sensibly uniform over the crystal for a spin refrigerator as well. Thus, we calculate p_{ss} by setting $\langle \bar{p}_n \rangle_i = p_{ni}{}^j = p_{ss}$ in Eq. (26) and set $\sum_j \delta p_n{}^j = 0$, then solve for p_{ss}. Replacing $\sum_j$ by $n \int d^3 r_j$, we find

$$p_{ss} = \frac{(4\pi n/3r_1{}^3)\langle C \rangle \tau p_{n0} + K_e \langle \langle \epsilon f_\epsilon \rangle \rangle \bar{p}_{es}}{(4\pi n/3r_1{}^3)\langle C \rangle \tau + [\langle \langle \epsilon^2 f_\epsilon \rangle \rangle - (1-K_e)\langle \langle \epsilon f_\epsilon \rangle^2 \rangle]}, \quad (28)$$

where now the double-averaged quantities $\langle \langle \epsilon f_\epsilon \rangle \rangle$, $\langle \langle \epsilon^2 f_\epsilon \rangle \rangle$, and $\langle \langle \epsilon f_\epsilon \rangle^2 \rangle$ are the cross-relaxation averages $\langle \epsilon f_\epsilon \rangle$, etc., averaged over the distribution of g values. Equation (28) depends on the proton concentration n but not the Yb concentration. This should be a valid prediction provided that the Yb concentration is neither so high that new cross- or spin-lattice-relaxation processes become important, nor so low that unwanted impurities significantly affect the proton spin-lattice relaxation time. If we multiply both numerator and denominator of Eq. (28) by $\gamma = N/n$ and recall that $(4\pi N/3r_1{}^3)\langle C \rangle = \langle C \rangle/(r_1 R)^3 = R_n$ as defined by LJ, we recognize that Eq. (28) is virtually identical to LJ's Eq. (40a) with these important differences: LJ's quantities ϵf, $\epsilon^2 f$ are replaced by quantities averaged so as to take into account both multiple-order cross-relaxation processes and the finite distribution of $g_\perp$ values. Also the right-most term in the denominator of Eq. (28) yields the entropy effect not recognized by LJ.

Other solutions to the diffusion equation may be required under different operating conditions. At higher operating speeds, or in other materials, it may happen that the scattering radius b exceeds r_1 by enough so that $\langle \bar{p}_n \rangle_i$ is determined by protons inside the scattering radius. These protons are mainly influenced by only one Yb spin, so that in the steady state, protons near the ith Yb spin have polarization

$$\langle \bar{p}_{ns} \rangle_i = \frac{(4\pi n/3r_1{}^3)\langle C \rangle \tau p_{n0} + K_e \langle \epsilon f_\epsilon \rangle_i \bar{p}_{es}}{(4\pi n/3r_1{}^3)\langle C \rangle \tau + \langle \epsilon^2 f_\epsilon \rangle_i - (1-K_e)\langle \epsilon f_\epsilon \rangle_i{}^2}. \quad (29)$$

The rest of the protons outside acquire the average

$$p_{ss} = \langle \langle \bar{p}_{ns} \rangle_i \rangle, \quad (30)$$

by spin diffusion, where again the outer set of brackets refers to an average over $g_\perp$ values. The expressions (29) and (30) are the result one would naively expect to obtain because of a distribution of $g_\perp$ values, but rapid spin diffusion implies that Eq. (28), a quite different type of average, should hold for the experiments reported here.

Buildup time. Calculation of the polarization buildup time is also analogous to the relaxation-time calculation. After several bulk spin-diffusion time constants (~ 1 sec) so that $p_n(\mathbf{r})$ has had time to become reasonably uniform, p_n approaches p_{ss} exponentially with buildup rate

$$\frac{1}{\tau_{0n}} = \frac{4\pi N}{3r_1{}^3}\langle C \rangle + \frac{N}{n}\frac{1}{\tau}[\langle \langle \epsilon^2 f_\epsilon \rangle \rangle - (1-K_e)\langle \epsilon f_\epsilon \rangle^2]. \quad (31)$$

Equation (31) is rather similar to LJ's Eq. (40b). If $b > r_1$, $\tau_{0n}{}^{-1}$ is reduced by the ratio $(r_1/b)^3$ by spin diffusion.

D. Polycrystalline Spin Refrigerator

For efficient operation of a pulsed-field spin refrigerator, cross-relaxation should occur in the tail of the pulse and the crystal should be so oriented that T_{1n} is large during the large fraction of a cycle that the pulse is off. These requirements dictate the use of well-

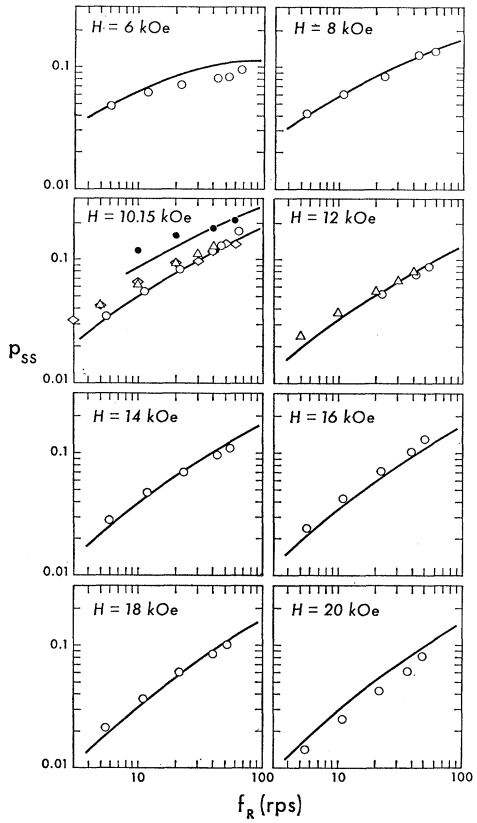

FIG. 13. Proton polarization p_{ss} versus f_R. Polycrystalline samples at $T=1.4$°K: ○, 2% ^{172}Yb:YES sample No. 18; ◇, 0.7% ^{172}Yb:YES sample No. 19; △, 0.7% ^{172}Yb:YES sample No. 20; ●, single crystal at $T=1.23$°K, crystal No. 9 of Ref. 2. The solid curves are Eq. (28).

oriented single crystals. In a rotating crystal spin refrigerator, crystal orientation is much less critical. For Yb:YES, the principal axes for $g_\perp$ lie in a plane, so

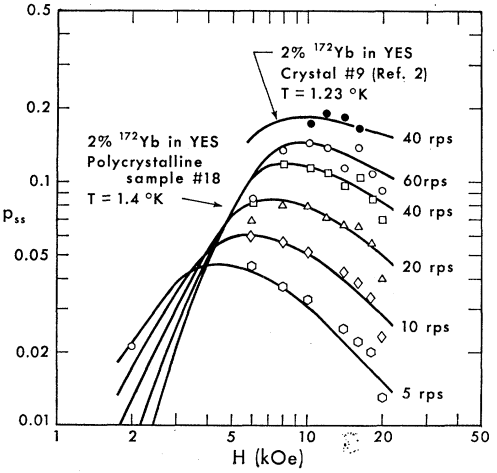

FIG. 14. Proton polarization p_{ss} versus H. Polycrystalline sample No. 18 at $T=1.4$°K; ○, $f_R=60$ rps; □, 40 rps; △, 20 rps; ◇, 10 rps; ⟨⟩, 5 rps. ●, single crystal, No. 18 (before grinding) at $T=1.18$°K. The solid curves are Eq. (28).

that cross-relaxation occurs whenever this plane contains **H**. The loss of polarization due to spin-lattice relaxation depends very little on orientation since the crystal continuously rotates. Thus it is entirely feasible to use polycrystalline samples in the rotating spin refrigerator; this may be a practical necessity in constructing large polarized targets for nuclear scattering since it is difficult to grow large, single crystals of YES.

When a polycrystalline sample is rotated in a field, each crystallite develops its own proton polarization. The observed proton polarization is the average $(p_{ss})_\psi = \int_0^{\pi/2} p_{ss}(\psi)\sin\psi d\psi$, where ψ is the angle made by the crystallite c axis and the rotation axis. In calculating $p_{ss}(\psi)$, we use easily derivable generalizations of Eq. (22), (23), and (B4a):

$$(\bar{p}_{es})_\infty(\psi) = \frac{32}{15\pi}\frac{g_{11}\mu_B H}{2kT}\sin\psi\left[\frac{1+4\cos^2\psi}{1+3\cos^2\psi}\right], \quad (32a)$$

$$(\bar{p}_{es})_0(\psi) = \Gamma(\tfrac{4}{3})\left[\frac{6\pi f_R \sin\psi}{AH^4T}\right]^{1/3}\frac{g_{11}\mu_B H}{2kT}, \quad (32b)$$

$$\dot{E}(\psi) = \dot{E}(\tfrac{1}{2}\pi)/\sin\psi, \quad (32c)$$

and the relations

$$K_e(\psi) = 1 - e^{-AH^4T\sin^2\psi(1+3\cos^2\psi)/16 f_R}, \quad (33a)$$

$$\langle C\rangle(\psi) = \sin^2\psi(1+3\cos^2\psi)\langle C\rangle(\psi=\tfrac{1}{2}\pi). \quad (33b)$$

VI. EXPERIMENTAL RESULTS AND INTERPRETATION

A. Proton Polarization in ^{172}Yb:YES Powder

LJ have reported extensive measurements of proton polarization in Yb:YES with Yb of natural isotopic abundance. We have repeated these measurements in LJ's apparatus for several polycrystalline samples of enriched ^{172}Yb:YES, over a range of fields $2000 \leqq H \leqq 20\,000$ Oe, rotation speeds $5 \leqq f_R \leqq 60$ rps and temperatures $1.2 \leqq T \leqq 1.8$°K. The samples used had a growing solution concentration of either 2% or 0.7% Yb:Y. We measured first the proton NMR signal proportional to $p_{n0}(H_0,T_0)$ at $H_0=10\,150$ Oe and $T_0=1.20$ K. Then we rotated the crystal at field H, and frequency f_R until the NMR signal reached a steady-state value proportional to $p_{ss}(f_R,H,T)$, where generally $T>T_0$ due to bearing friction. The NMR signals were measured by switching the field back to 10 150 Oe and measuring the peak of the absorption signal on an oscilloscope; field switching and NMR measurement take less than 5 sec, much less than $T_{1n}\sim 300$ sec at this field.

The results are shown in Fig. 13 as a plot of observed proton polarization p_{ss} versus f_R at various magnetic fields; the data are also cross-plotted in Fig. 14 to show p_{ss} versus H for constant f_R.

The solid curve in Figs. 13 and 14 is Eq. (28), suitably averaged for a polycrystalline sample, using $n=5.6\times10^{22}$

protons/cm^3 and $r_1=3.1$ Å. There are only two unknown parameters left: A', the direct process coefficient is needed for calculating K_e, $\bar{p}_{es}$, and $\langle C\rangle$; and g_0, the width of the distribution of $g_\perp$ in Eq. (9), is needed in order to calculate $\langle\langle\epsilon^2 f_\epsilon\rangle\rangle$, etc. We have chosen these parameters by least-squares fitting Eq. (28) to our data using an IBM 7094-7040 computer. The best values are $A'=8\times10^{-17}$ Oe^{-5} sec^{-1} and $g_0=0.003$ which turns out, fortuitously, to be very near g_n. This value of A' is 1.7 times lower than LJ's calculated value, but 2.5 times higher than the value they determined from their proton relaxation results; g_0 is just at the lower limit of the range if values we estimated in Sec. III B.

Data on a single crystal of 2% ^{172}Yb:YES reported by LJ and data taken by us on crystal No. 18 before it was ground to a powder are also plotted in Figs. 13 and 14, respectively. The solid curves are also Eq. (28), for a single crystal.

The excellent agreement between the solid curves and data points in Figs. 13 and 14 is encouraging evidence that the over-all theory in Sec. V is not far wrong. The theory would be on firmer ground if A' could be measured. This appears to be extremely difficult experimentally. If we assume that the theory is correct, it is interesting to extrapolate the calculations to higher frequencies; in Fig. 15 we show calculated values of $(p_{ss})_\psi$ for polycrystalline Yb:YES at $T=1.15$°K, obtainable by pumping liquid helium, at frequencies up to $f_R=2000$ rps. The extrapolation is not entirely trustworthy because we have neglected the adiabatic passage effects mentioned in the previous section as well as the alternate solution to the spin-diffusion equation. Nevertheless, our predicted valued $p_{ss}=75\%$ at $H=20\,000$ Oe and $f_R=2000$ rps indicates the very interesting potential of the spin refrigerator as a device for producing polarized targets. Sample rotation speeds up to $f_R=300$ rps may actually be practical, yielding $p_{ss}=40\%$; above this speed, it may be simpler to rotate the field rather than the crystals.

The effective number of protons which flip for each Yb spin flip can be defined by $\epsilon_{\rm eff}=\langle\epsilon^2 f_\epsilon\rangle/\langle\epsilon f_\epsilon\rangle$. From Eq. (28) we see that at high enough operating speeds (i.e., $\tau\to0$) so that nuclear spin-lattice relaxation can be neglected, but low enough so that the entropy effect is insignificant ($K_e\approx1$), we see that $p_{ss}\to\bar{p}_{es}/\epsilon_{\rm eff}$, so that $\epsilon\sim1$ is desirable. We plot calculated values of $\epsilon_{\rm eff}$ versus H in Fig. 16. The plot shows that high fields and frequencies lead to the smallest values of $\epsilon_{\rm eff}$, as found empirically by LJ.

The agreement between theory and our data for both single-crystal and polycrystalline samples, and LJ's data on enriched ^{172}Yb single crystals is rather satisfying. However, while our theory predicts no effects due to Yb hyperfine structure, it is abundantly evident from LJ's results that crystals with natural abundance of Yb isotopes produce substantially lower proton polarizations than the enriched crystals. A tentative explanation of this decrease is that cross-relaxation with protons

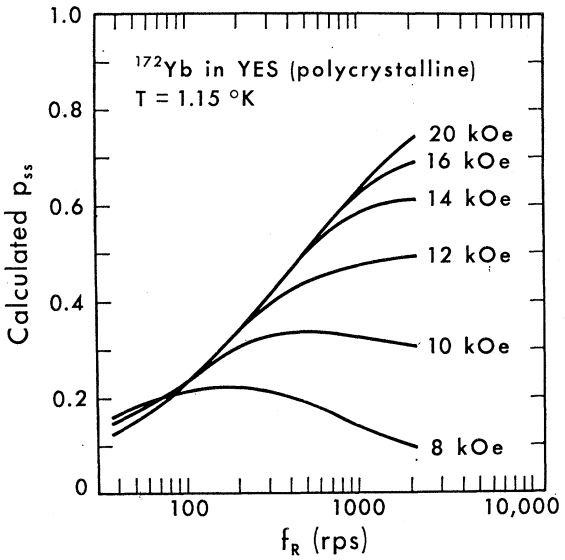

FIG. 15. Calculated proton polarization [Eq. (28)] extrapolated to high frequencies for polycrystalline ^{172}Yb:YES.

occur at different times for Yb spins with and without hyperfine structure, respectively, because the two types of spin have different effective local fields, as explained in Sec. II B. The first Yb spin to cross-relax with protons is warmed to the proton spin temperature; midway between, the two Yb spins are on speaking terms, so that Yb-Yb cross-relaxation pre-warms the

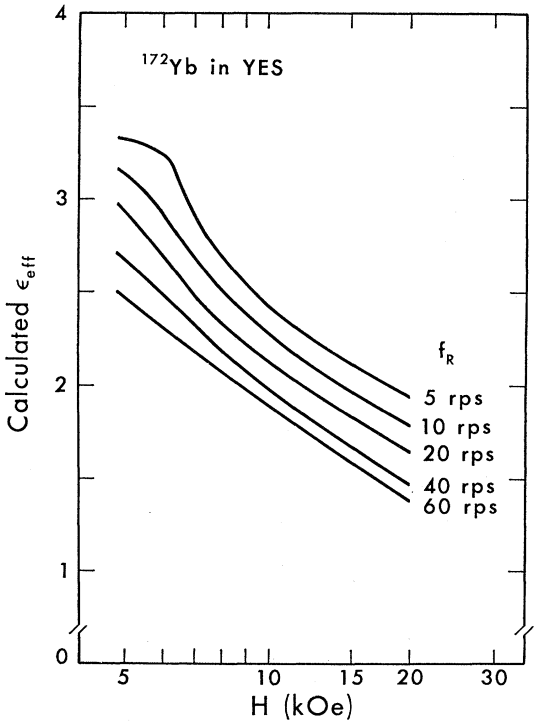

FIG. 16. Plot of $\epsilon_{eff}=\langle\epsilon^2 f_\epsilon\rangle/\langle\epsilon f_\epsilon\rangle$ versus H for various f_R, showing $\epsilon_{eff}\to1$ at high H and f_R.

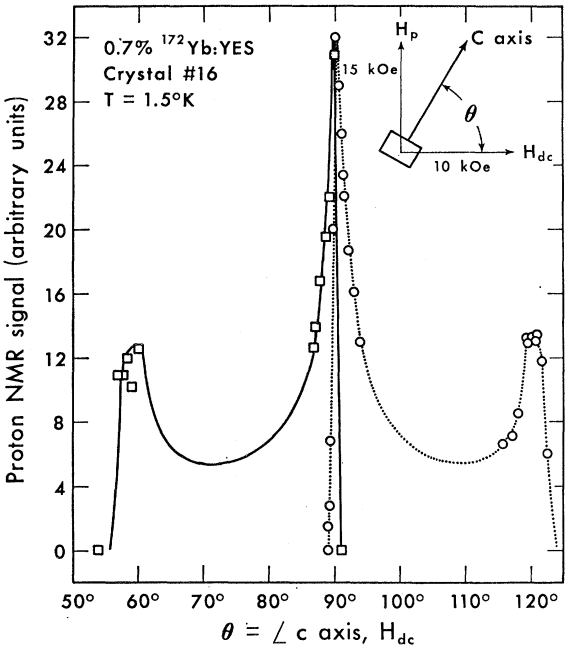

FIG. 17. Dependence of proton polarization after 30 sec in pulsed field spin-refrigerator on orientation of single crystal. □, H_{dc} in "normal" direction. ○, H_{dc} in "reverse" direction. Pulse shape is shown in Fig. 5(c).

second Yb spin before it can cross-relax with its protons. Thus, a fraction of the Yb spins which is roughly the fraction h which have hyperfine structure are prevented from cooling protons, and, in fact, warm them up by cross-relaxation. This fraction is also not prevented from warming protons by spin-lattice relaxation during the rest of the cycle, so the resulting proton polarization may be reduced by a factor $1-h$. Since $h=2\%$ for our enriched samples, we can safely neglect this effect; but $h=30\%$ for natural Yb, so a reduction by 0.7 would not be unreasonable. The observed ratio is actually roughly 0.5, in fair agreement with our tentative explanation.

Polarization buildup times. Buildup times for p_{ss} were not measured exactly for crystal No. 18, but at $f_R=60$ rps, $H=10$ kOe, p_n reaches steady state typically in less than 3 min, indicating an exponential buildup time less than 1 min. This is consistent with $\tau_{0n}=25$ sec calculated from Eq. (31) using Yb concentration $c=0.6\%$. For crystal No. 19 (0.7% ^{172}Yb:YES) at 12 000 Oe, we measure $\tau_{0n}=297$ sec at $f_R=10$ rps and $\tau_{0n}=455$ sec at $f_R=5$ rps. Assuming the rejection ratio 0.3 determined for 2% crystals, the actual concentration is 0.21%, and we calculate $\tau_{0n}=230$ and 310 sec, respectively, from Eq. (31). The agreement is not unreasonable, but there is unfortunately not enough data available to test for diffusion effects or any other breakdown of our model.

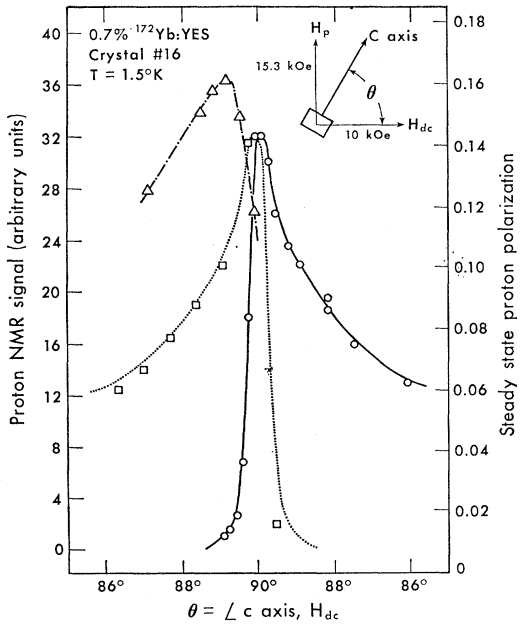

FIG. 18. Proton polarization in pulsed-field spin-refrigerator. □,○, NMR signal after 30-sec pulsing for H_{dc} in normal, reversed direction, respectively. Δ, steady-state proton polarization for H_{dc} in normal direction. Pulsed-field shape is shown in Fig. 5(c).

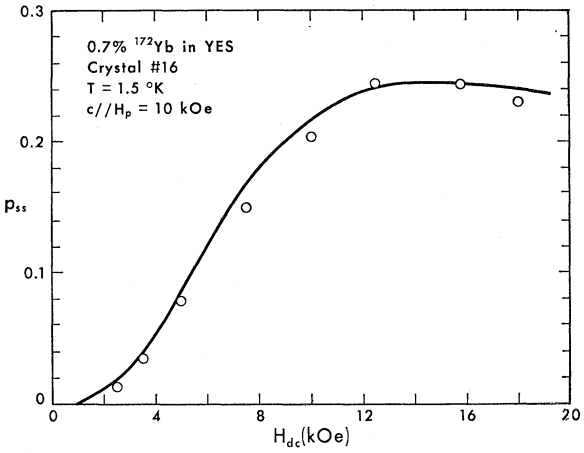

FIG. 19. Steady-state proton polarization p_{ss} versus H_{dc} for pulsed-field spin refrigerator. Pulse shape is shown in Fig. 5(c). The field pulses have magnitude 10 kOe and repetition rate 20 pps. The solid curve is Eq. (28) as explained in text.

B. Pulsed-Field Spin Refrigerator

Proton polarization measurements were made for a pulsed-field spin refrigerator with the two pulse shapes of Figs. 5(a) and 5(c). When using the trapezoidal-pulse shape of Fig. 5(c), a single crystal of ^{172}Yb:YES was mounted in a rotatable crystal holder so that the crystal could be rotated in a vertical plane containing the crystalline c axis, $\mathbf{H}_{dc}$, and $\mathbf{H}_p$.

After measuring the thermal equilibrium proton NMR signal proportional to p_{n0}, the crystal was accurately aligned using the spin-refrigerator effect itself. The field is pulsed on for a time t short compared to τ_{0n},

so that the protons acquire polarization $[t/\tau_{0n}(\theta)]p_{ss}(\theta)$, where θ is still the angle between $\mathbf{H}_{dc}$ and the c axis. A typical result is shown in Fig. 17, with $H_{dc}=15.3$ kOe showing clearly that cross-relaxation between proton and Yb spins occurs most efficiently either in the tail of the pulse when $\theta\approx 90°$, or in the flat peak of the pulse at $\theta=57°$. The latter measurement shows that $H_{p,\max}=H_{dc}\cot 57°=10.0$ kOe, verifying our measurement of H_p with the integrated output of a pickup coil. Figure 17 also gives the results of the same experiment in which $\mathbf{H}_{dc}$ is reversed. The symmetry between the two curves is used to orient the crystal accurately.

In Fig. 18, we present the data of Fig. 17 with an expanded scale about $\theta=90°$. We also present the final steady-state polarization as a function of angle in the same figure. This figure shows that the highest proton polarization is obtained when cross-relaxation occurs just before the pulse is turned off, in the exponentially decaying tail of the field pulse. The reason for this is that cross-relaxation while the pulsed field is off acts as a source of leakage relaxation for the protons, as shown in LJ's Fig. 12.

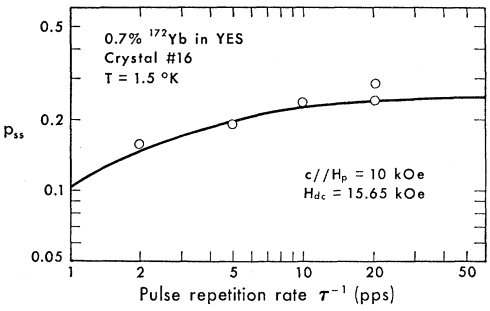

FIG. 20. Steady-state proton polarization p_{ss} versus pulse repetition rate τ^{-1} for pulsed-field spin refrigerator. Pulse repetition in pulses per second (pps). Pulse shape is shown in Fig. 5(c). $H_p=10$ kOe. The solid curve is Eq. (28) as explained in text.

From Fig. 18 we determine that the optimal orientation for achieving the highest p_{ss} is $\theta=89°$, so that the pulsed-field strength during cross-relaxation is $H_0=H_{dc}\tan 1°=0.0175H_{dc}$, to be used in Eq. (B4b). Comparing to Eq. (B4a) we find that the value of $\dot{E}$ is equivalent to that for a rotating crystal spin refrigerator with $f_R=10$ rps. Thus, the Yb polarization $\bar{p}_{es}$ is determined by rapid switching of the field pulse corresponding to $\sim 2kHz$, but the proton polarization is determined by cross-relaxation corresponding to a much slower rotation speed, making the pulsed-field spin refrigerator much more efficient than the rotating crystal type.

Figure 19 shows measured values of p_{ss} versus H_{dc} obtained for 0.7% ^{172}Yb:YES crystal No. 16, with 10-kOe trapezoidal-pulses and repetition rate $\tau^{-1}=20$ pulses/sec, the fastest rate our apparatus would permit. The crystal was oriented so that $\theta=89°$ with respect to $\mathbf{H}_{dc}$. The solid curve is Eq. (28) with $\langle C\rangle$ given by Eq. (14) and T_{1e}^{-1} given by the Raman process relaxation rate determined by LJ. The parameters $\langle\langle\epsilon^2 f_\epsilon\rangle\rangle$ and $\langle\langle\epsilon f_\epsilon\rangle\rangle$ are taken from the calculations of Figs. 14 and 15 for a rotating crystal spin-refrigerator at $f_R=10$ rps. Values of $\bar{p}_{es}$ were interpolated from Fig. 11 using $A'=8\times 10^{-17}$ Oe^{-5} sec^{-1}, the value determined in the previous section.

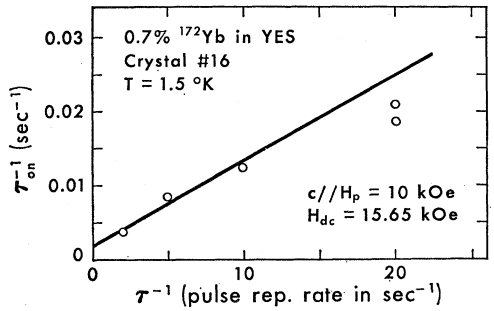

FIG. 21. Proton polarization buildup rate τ_{0n}^{-1} versus pulse repetition rate τ^{-1} for the data of Fig. 20. The solid curve is Eq. (41).

Figure 20 presents the repetition rate dependence of p_{ss} at $H_{dc}=15.6$ kOe, everything else being the same as in Fig. 19. Again the solid curve is Eq. (28), calculated as above.

The excellent agreement between the calculated curves and experimental results is further evidence that the analysis of Sec. V is essentially correct.

Buildup times. Figure 21 shows the buildup rate τ_{0n}^{-1} versus the pulse rate τ^{-1}, observed for the polarization measurements of Fig. 20. The solid curve is Eq. (31) calculated using Yb concentration of 0.21% which we obtain by assuming the Yb rejection ratio is the same as for crystals grown from the 2% Yb:YES growing solution. The agreement between theory and experiment is as good as can be expected since solutions to the spin-diffusion equation do not yet agree exactly even with nuclear spin-lattice relaxation rates.

Additional experiments were performed using the "half-sine" pulse shape of Fig. 5(a). This pulse shape is less ideal than the "trapezoidal" pulse shape of Fig. 5(c) but higher field strengths can be produced for the same

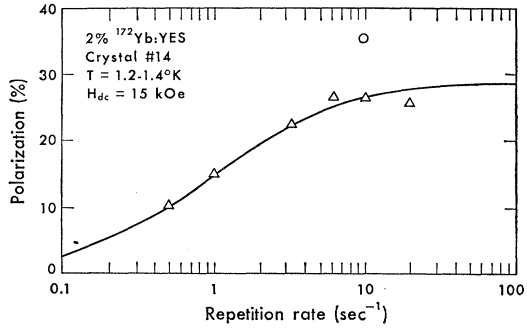

FIG. 22. Steady-state proton-polarization p_{ss} versus pulse repetition rate τ^{-1} for pulsed-field spin-refrigerator. The pulse shape is shown in Fig. 5(a). △, $H_p=15$ kOe. ○, $H_p=$kOe. The solid curve is Eq. (3) of Ref. 17.

capacitor bank energy. Thus we were able to operate 15-kOe half-sine pulses at 20 pulses/sec rather than only 10-kOe trapezoidal pulses. This resulted in higher values of p_{ss} as shown in Fig. 22. The apparatus can also produce 20-kOe pulses at the lower pulse rate 10 pps; with this configuration we observed our highest proton polarization, $p_{ss}=35\%$, briefly reported earlier.[17] The solid curve in Fig. 22 is that calculated in Ref. 17 from a tentative theory involving only 1:1 spin flips.

C. Polarization of Deuterons

We have also used the spin refrigerator to polarize deuterons. Crystal No. 17 (1% ^{172}Yb in YES) was grown by dissolving a Yb:YES crystal in pure D_2O and regrowing new crystals with fresh dry desiccant, repeating the process five times. We estimate that approximately 80% of the protons of the water of hydration are replaced by deuterons, but the protons of the ethyl radicals are not replaced.

A maximum deuteron polarization of 0.6% was measured in both types of spin refrigerator, operated at their maximum speeds of 60 rps and 20 pulses/sec, respectively, for rotation and trapezoidal-field pulsing. This low nuclear polarization is due to the small value of the deuteron g_n factor, which is 6.7 times smaller than for protons. This means both that only a small fraction of the Yb spins can participate in low-order cross-relaxation processes, and that the protons remaining in the crystal cross-relax with the Yb spins first, warming them up before Yb-deuteron cross-relaxation can occur. The second problem can be overcome by using completely deuterated crystals. The first problem would be less important at higher rotation speeds, so it may still be possible to achieve high deuteron polarizations using spin refrigerators.

VII. SUMMARY AND CONCLUSIONS

By subjecting a single crystal of 2% ^{172}Yb:YES to a combination of 200-μsec pulsed fields $\mathbf{H}_p=20$ kOe and static fields $\mathbf{H}_{dc}=15$ kOe at $T=1.2$°K, we have obtained proton spin polarizations up to 35%. We have also obtained proton polarizations up to 16% in polycrystalline 0.7% ^{172}Yb:YES simply by rotating the sample at $f_R=60$ rps in a field $H=10$ kOe at $T=1.4$°K. Both types of experiments are well-explained by a unified theory of spin-refrigerators involving detailed investigation of spin-diffusion, spin-lattice, and cross-relaxation processes. The new theory predicts even higher proton polarizations, up to 70% by sample rotation at higher speeds $f_R\sim2000$ rps and higher fields $H\sim20$ kOe.

Polycrystalline samples may be used. The magnetic field need not be very homogeneous, and the average heat loss to the liquid helium bath can be made small. Yb:YES is 5.3% hydrogen by weight compared to 3% for Nd:LMN used in the microwave dynamic-polarization method. All of these suggest that use of Yb:YES and the spin-refrigerator method may be of practical importance in constructing polarized proton targets. The optimum configuration still cannot be specified. Equipment to rotate the field rather than the crystal is now being constructed at Berkeley by R. L. Ballard.

ACKNOWLEDGMENTS

We acknowledge with pleasure the essential help of K. H. Langley in many phases of this work; many discussions with R. L. Ballard on the theory of the spin refrigerator; and useful discussions with R. Orbach and R. J. Birgeneau on phonon-induced g shifts.

APPENDIX A

Consider a system of coupled Yb spins and proton spins, in which there are N per cm^3 Yb spins S^i, each having population $\frac{1}{2}(1-p_e{}^i)$ and $\frac{1}{2}(1+p_e{}^i)$ in the upper and lower energy levels, respectively, interacting with n per cm^3 proton spins I^j, with populations $\frac{1}{2}(1-p_n{}^j)$ and $\frac{1}{2}(1+p_n{}^j)$ in the upper and lower levels, respectively. The cross-relaxation rate equations for this system are easily shown to be

$$\dot{p}_n{}^j=\sum_i W_{ij}[p_e{}^i-p_n{}^j], \tag{A1a}$$

$$\dot{p}_e{}^i=\sum_j W_{ij}[p_n{}^j-p_e{}^i], \tag{A1b}$$

where W_{ij} is the transition probability for a flip-flop between the ith Yb spin and jth proton spin. These equations couple together the polarization of every spin in the crystal, i.e., they are actually a set of $\approx10^{22}$ coupled simultaneous equations, so that an exact solution is impossible. An approximate solution can be realized, however: We solve Eq. (A1b) first, assuming that the $p_n{}^j$ are constants equal to $\bar{p}_n{}^j$, the proton polarizations at the *end* of the lattice relaxation part of the cycle. This is approximately correct because the protons outnumber Yb spins by so much that individual protons experience only a small change in polarization. The appropriate solution to Eq. (A1b) is[2]

$$p_{ef}{}^i(t)=\left\{\exp\left[-\int_{t_0}^{t}\sum_j W_{ij}\cdot dl\right]\right\}\times\left\{\int_{t_0}^{t}\exp\left[\int_{t_0}^{t'}\sum_j W_{ij}\cdot dt''\right]\times\left(\sum_j W_{ij}\bar{p}_n{}^j\right)dt'+\bar{p}_e{}^i\right\}, \tag{A2}$$

where $p_{ef}{}^i$ is the polarization of the ith Yb spin *after* the cross-relaxation cycle. The integrals are taken over the cross-relaxation cycle time $t-t_0=\tau_2$. The second integral in Eq. (A2) is evaluated by making the

substitution

$$q_{ij}(t)=\int_{t_0}^{t} W_{ij}(t')dt'. \tag{A3}$$

The result is

$$p_{ef}{}^{i}(t)=(1-f_1{}^{i})\bar{p}_e{}^{i}+f_1\langle\bar{p}_n\rangle_i, \tag{A4a}$$

where

$$f_1{}^{i}=1-\exp[-\sum_j q_{ij}(\tau_2)], \tag{A4b}$$

is the probability to complete 1:1 cross-relaxation, and $\langle\bar{p}_n\rangle_i=\sum_j q_{ij}(\tau_2)\bar{p}_n{}^{j}/\sum_j q_{ij}(\tau_2)$ is the weighted average proton polarization felt by the ith Yb spin. It is fortunate that Eq. (A4) contains only integrals of W_{ij}, because these integrals turn out to be easy to calculate, even though the cross-relaxation rates W_{ij} themselves are extremely difficult to calculate.[48] From the golden rule of time-dependent perturbation theory,

$$W_{ij}=\frac{2\pi}{\hbar}|V_{ij}|^2\rho_{ij}(E), \tag{A5}$$

where V_{ij} is the matrix element of the Yb-proton magnetic-dipole–dipole Hamiltonian for simultaneously flipping both spins, and $\rho_{ij}(E)$ is the density of final states which conserve total energy when the Zeeman energy mismatch is E. Equation (A5) cannot be evaluated directly, because $\rho_{ij}(E)$ is not well enough known. Nevertheless, for a linear level crossing, $E(t)\approx E(t_0)+\dot{E}\times(t-t_0)$, so that the substitution $dt=dE/\dot{E}$ can be made. It is also certainly true that $\rho_{ij}(E)$ varies much faster with E than $|V_{ij}|^2$, so that

$$q_{ij}(\tau_2)=\int_{t_0}^{t_0+\tau_2}\frac{2\pi}{\hbar}|V_{ij}(E)|^2\rho_{ij}(E)dt$$

$$\approx\frac{2\pi}{\hbar}|V_{ij}(0)|^2\int_{-\infty}^{\infty}\frac{\rho_{ij}(E)dE}{\dot{E}}=\frac{2\pi|V_{ij}|^2}{\hbar\dot{E}}. \tag{A6}$$

The limits of integration have been extended to $\pm\infty$ because $\rho_{ij}(E)$ is zero at the beginning and end of the cross-relaxation cycle.

We now solve Eq. (A1a) for the proton polarization, replacing $p_e{}^{i}$ by our solution to Eq. (A1b). Neglecting second order effects due to Yb-aided proton-proton spin flips, which are only a small contribution to proton-spin diffusion, we find that $p_{nf}{}^{j}$, the proton polarization at the end of the cycle is

$$p_{nf}{}^{j}=\bar{p}_n{}^{j}+\sum_i\{q_{ij}f_1{}^{i}[\bar{p}_e{}^{i}-\langle\bar{p}_n\rangle_i]/\sum_k q_{ik}\}. \tag{A7}$$

Since $q_{ij}\propto|V_{ij}|^2\propto r_{ij}^{-6}$, protons very near Yb ions experience the largest change in polarization, as expected.

[48] W. J. C. Grant, Phys. Rev. **134**, A1554 (1964); **134**, A1565 (1964); **134**, A1574 (1964); **135**, A1265 (1964).

APPENDIX B

For the general ϵ:1 cross-relaxation process, in which ϵ proton sflip while one Y bspin flops, Eqs. (A4a) and (A7) become, in the high-temperature approximation,

$$p_{ef}{}^{i}=(1-f_\epsilon{}^{i})\bar{p}_e{}^{i}+\epsilon f_\epsilon\langle\bar{p}_n\rangle_i, \tag{B1a}$$

$$p_{nf}{}^{j}=\bar{p}_n{}^{j}+\sum_i\{q_{ij}[\epsilon f_\epsilon{}^{i}\bar{p}_e{}^{i}-\epsilon^2 f_\epsilon\langle\bar{p}_n{}^{j}\rangle_i]/\sum_k q_{ik}\}, \tag{B1b}$$

where f_ϵ is the cross-relaxation probability for ϵ:1 spin flips, to be calculated as in Eqs. (A4) and (A6) but using ϵth-order time-dependent perturbation theory.

Equations (B1) are still not yet the result we seek, for they are correct only if *one* process involving ϵ proton spins and one Yb spin occurs. Actually, all orders of cross-relaxation occur, but in a definite order. As the field is rotated through 90°, the Yb spin-energy splitting first decreases, reaches a minimum at $g=g_\perp$, then increases again. Thus, cross-relaxation processes occur in the order $\{\cdots\rightarrow 3{:}1\rightarrow 2{:}1\rightarrow 1{:}1\rightarrow\theta=90°\rightarrow 1{:}1\rightarrow 2{:}1\rightarrow 3{:}1\rightarrow\cdots\}$. We have calculated the polarizations resulting from all these cross-relaxation processes by using the final polarizations at the end of the 3:1 process as the initial polarizations at the beginning of the 2:1 process, etc. Taking into account all processes up to $\epsilon=3$, we find that the resulting polarizations can be expressed in the form of Eqs. (B1), but that the quantities ϵf_ϵ, $\epsilon^2 f_\epsilon$ and $(1-f_\epsilon)$ are replaced by effective averages:

$$\langle\epsilon f_\epsilon\rangle=3f_3+(1-f_3)\{2f_2+(1-f_2)\times[f_1'+(1-f_1')(2f_2+(1-f_2)3f_3)]\}, \tag{B2a}$$

$$\langle\epsilon^2 f_\epsilon\rangle=18f_3+8f_2+f_1'-12f_3f_3-6f_1'f_3(1-f_2)-4f_1'f_2-12f_2f_3(1-f_1')(1-f_2)-4f_2{}^2(1-f_1')-9f_3{}^2(1-f_2)^2(1-f_1'), \tag{B2b}$$

$$\langle 1-f_\epsilon\rangle=(1-f_3)^2(1-f_2)^2(1-f_1'), \tag{B2c}$$

where $(1-f_1')=(1-f_1)^2$. From Eq. (B1b) the polarization of the jth proton due to the ith Yb spin tends towards $p_n{}^{j}\rightarrow\bar{p}_{es}[\langle\epsilon f_\epsilon\rangle/\langle\epsilon^2 f_\epsilon\rangle]$. This becomes $\bar{p}_{es}/\epsilon$ if one process occurs with finite probability. When multiple spin-flip processes occur, there is a quite unusual effect. For example, when $f_3=f_2=f_1=1$, all these cross-relaxation processes are complete and $\langle\epsilon f_\epsilon\rangle=3$, but $\langle\epsilon^2 f_\epsilon\rangle=11$, so that $p_n{}^{j}\rightarrow(3/11)\bar{p}_{es}$, rather than $1/3\bar{p}_{es}$, the result when *only* 3:1 processes occur. Thus, 2:1 and 1:1 spin-flip processes actually can slightly lower the proton polarization, even though acting alone they produce higher polarization than 3:1 processes. This effect has a simple thermodynamic interpretation: Each cross-relaxation process can be thought of as thermal mixing between two thermal reservoirs. The final 3:1 process determines the final proton spin temperature regardless of whether or not it was preceded by 1:1 and 2:1 processes. Nevertheless, from the second law of thermodynamics, every thermal mixing raises

the entropy of the system, so that the final spin temperature is higher because of increased entropy when 2:1 and 1:1 flips precede the 3:1 process. This is a fairly minor effect except at very high operating speeds such that $K_\epsilon \ll 1$, so that the increase in spin temperature due to the entropy effect dominates the cooling of the spin refrigerator effect.

Calculation of completeness coefficients. Equations (A4) and (A6) are easily generalized to calculate f_ϵ simply by using ϵ-order time-dependent perturbation theory. Of course, for 2:1 spin flips, the sum over protons in Eq. (A6) becomes a sum over *pairs* of protons, and so forth for higher-order processes. The relevant part of the Yb-proton dipole-dipole Hamiltonian has been given previously[39]:

$$V_{ij}=g_n\frac{g_{\parallel}\mu_B{}^2}{r_{ij}{}^3}\left(\frac{1-3\cos^2\Theta_{ij}+3\sin^2\Theta_{ij}e^{-2i\Phi_{ij}}}{8}\right)\times\{4[1-(g_\perp/\epsilon g_n)^2]^{1/2}S_z{}^iI_+{}^j+(g_\perp/\epsilon g_n)S_+{}^iI_+{}^j\}+\text{H.c.}, \quad \text{(B3)}$$

where $(r_{ij},\Theta_{ij},\Phi_{ij})$ is the position of the jth proton w.r.t. the ith Yb^{3+} ion.

We have given the S_+I_+ part of the dipole-dipole Hamiltonian for flipping both spins, rather than S_+I_- and S_-I_+ terms, because the gyromagnetic ratios of protons and electrons have opposite signs, so their angular momenta flip in the same direction when their magnetic moments flip in opposite directions. Actually, the relative sign of g for Yb spin and protons is of no importance here, because at the angle where $|g(\theta)|=g_n$ the coefficient of the S_-I_+ term is precisely equal to the coefficient of the S_+I_+ term. This, of course, untrue for isotropic spins.

The rates of change of Zeeman energy mismatch are easily shown to be

$$\dot{E}=2\pi f_R[1-(g_\perp/\epsilon g_n{}^2)]^{1/2}g_{\parallel}\mu_B H\,, \quad \text{(B4a)}$$

$$\dot{E}=[1-(g_\perp/\epsilon g_n)^2]^{1/2}g_{\parallel}\mu_B H_0/\tau_0\,, \quad \text{(B4b)}$$

for rotating crystal- and pulsed-field spin refrigerators, respectively, where H_0 is the magnitude of the pulsed field at the instant that cross-relaxation occurs and τ_0 is the decay time constant of the field pulse.

We have calculated f_ϵ for $\epsilon=1$, 2, and 3 by performing lattice sums for the 123 protons inside an 8 Å sphere about a Y site. The results for a rotating-crystal spin refrigerator are:

$$f_1=1-\exp\left\{\frac{-4.08\times10^7(g_\perp/g_n)^2}{[1-g_\perp^2/g_n^2]^{1/2}f_RH}\right\}, \quad \text{(B5a)}$$

$$f_2=1-\exp\left\{-6.38\times10^{13}\left(\frac{g_\perp}{g_n}\right)^2\times\frac{[1-(g_\perp/2g_n)^2]^{1/2}}{f_RH^3}\right\} \quad \text{(B5b)}$$

$$f_3=1-\exp\left\{\frac{-(g_\perp/g_n)^2}{f_RH^5[1-g_\perp{}^2/9g_n{}^2]^{1/2}}\times\left[6.15\times10^{19}\left(1-\frac{g_\perp{}^2}{9g_n{}^2}\right)^2+4.84\times10^{17}\left(1-\frac{g_\perp{}^2}{9g_n{}^2}\right)\left(\frac{g_\perp}{g_n}\right)^2+4.23\times10^{15}\left(\frac{g_\perp}{g_n}\right)^4\right]\right\}. \quad \text{(B5c)}$$

For the specific values $H=20\,000$ Oe, $g_\perp=\frac{1}{2}g_n$, and $f_R=60$ rps, these formulae yield $f_1=1$, $f_2=0.032$, and $f_3=0.0001$, showing that the 1:1 process dominates at the highest field and rotation speed permitted by our equipment. However, for $H=6000$ Oe, $g_\perp=\frac{1}{2}g_n$, and $f_R=5$ rps, the results are $f_1=1$, $f_2=1$, and $f_3=0.32$, showing that all three processes are important at lower fields and frequencies. Equations (B5) can also be used for pulsed-field spin refrigerators. From Eq. (B4) we calculate an effective rotation speed $f_R=H_0/(2\pi\tau_0H)$ to be used in Eq. (B5).